

ADA047986

AIRCRAFT RESPONSE EFFECT
ON E-FIELD MEASUREMENTS

R & D Associates
4640 Admiralty Way
Marina del Rey, California 90291

9 March 1977

Topical Report

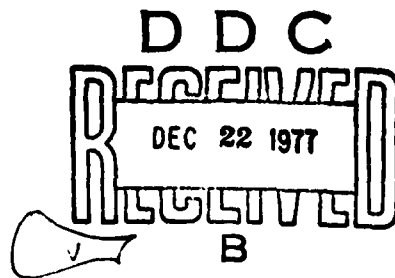
CONTRACT No. DNA 001-77-C-0012

APPROVED FOR PUBLIC RELEASE;
DISTRIBUTION UNLIMITED.

THIS WORK SPONSORED BY THE DEFENSE NUCLEAR AGENCY
UNDER RDT&E RMSS CODE B310077464 P99QAXDB00124 H2590D.

Prepared for
Director
DEFENSE NUCLEAR AGENCY
Washington, D. C. 20305

NO. 1
DDC FILE COPY
300



(18) DNA, SBIE
UNCLASSIFIED

SECURITY CLASSIFICATION OF THIS PAGE (When Data Entered)

(19) REPORT DOCUMENTATION PAGE		READ INSTRUCTIONS BEFORE COMPLETING FORM
1. REPORT NUMBER DNA 4279T AD-E300 Q42	2. GOVT ACCESSION NO.	3. RECIPIENT'S CATALOG NUMBER
4. TITLE (and Subtitle) AIRCRAFT RESPONSE EFFECT ON E-FIELD MEASUREMENTS	5. TYPE OF REPORT & PERIOD COVERED Topical Report	6. PERFORMING ORG. REPORT NUMBER RDA-TR-140801-008
7. AUTHOR(s) Gerard K. Schlegel	8. CONTRACT OR GRANT NUMBER(s) DNA 001-77-C-0012	9. PROGRAM ELEMENT, PROJECT, TASK AREA & WORK UNIT NUMBERS Subtask P99QAXDB001-24
10. CONTROLLING OFFICE NAME AND ADDRESS Director Defense Nuclear Agency Washington, D.C. 20301	11. REPORT DATE 9 March 1977	12. NUMBER OF PAGES 88
13. MONITORING AGENCY NAME & ADDRESS (if different from Controlling Office) (19) 800.	14. SECURITY CLASS (of this report) UNCLASSIFIED	15a. DECLASSIFICATION/DOWNGRADING SCHEDULE
16. DISTRIBUTION STATEMENT (of this Report) Approved for public release; distribution unlimited.		
17. DISTRIBUTION STATEMENT (of the abstract entered in Block 20, if different from Report)		
18. SUPPLEMENTARY NOTES This work sponsored by the Defense Nuclear Agency under RDT&E RMSS Code B310077464 P99QAXDB00124 H2590D.		
19. KEY WORDS (Continue on reverse side if necessary and identify by block number) Antenna Effective Height Electric Field Measurements CW Phase Calculations		
20. ABSTRACT (Continue on reverse side if necessary and identify by block number) This report describes the effect of the aircraft response on the measurement of E-fields. In investigating this effect, the effective height data developed by the Boeing Corporation for a 1-m blade antenna on a C-130 aircraft was utilized. Difficulties in using this data are discussed, and calculated phase functions to correspond to the amplitude data are presented. Calculated antenna open circuit voltages are then presented for different free field variations and polarizations.		

PREFACE

We wish to acknowledge the valuable suggestions and critical discussions provided by W. J. Karzas during the performance of this study.

ACCESSION for	
NTIS	White Section <input checked="" type="checkbox"/>
DDC	Buff Section <input type="checkbox"/>
UNANNOUNCED <input type="checkbox"/>	
JUSTIFICATION _____	
BY _____	
DISTRIBUTION/AVAILABILITY CODES	
Dist.	AVAIL. and / or SPECIAL
A	

TABLE OF CONTENTS

<u>Section</u>		<u>Page</u>
I	Introduction	7
II	Aircraft Response Transfer Functions	9
	2.1 Vertical Effective Height	10
	2.2 Horizontal Effective Height	14
III	Effect of Aircraft Response on Measurements	23
	3.1 Vertical Polarization Effects	27
	3.2 Horizontal Polarization Effects	27
	3.3 30° Polarized Field	33
IV	Conclusion	36
Appendices		
A	Relationships between Phase and Amplitude Under Causality Constraint	39
B	Difficulties in Using the Boeing Effective Height Data	55
C	Effective Heights for Antennas on Conducting Surfaces	75

LIST OF FIGURES

<u>Figure</u>		<u>Page</u>
<u>Aircraft Response Transfer Functions</u>		
1a	$h_e(t)$ for Vertically Polarized Data	11
1b	$h_e(t)$ for Horizontally Polarized Data	11
2	$ h_e(\omega) $ for Vertical Electric Field	12
3	Phase of $h_e(\omega)$ for a Vertical Electric Field	15
4	Delta Function Response for Vertical Polarization . .	16
5	Step Function Response for Vertical Polarizations . .	17
6	$ h_e(\omega) $ for a Horizontal Electric Field	18
7	Phase of $h_e(\omega)$ for a Horizontal Electric Field . . .	20
8	Delta Function Response for Horizontal Polarization .	21
9	Step Function Response for Horizontal Polarization .	22
<u>Effect of Aircraft Response on Measurements</u>		
10	Time Waveform of the Incident Electric Field	24
11a	$ E(\omega) $ for the Incident Electric Fields	25
11b	Phase for the Incident Electric Fields	26
12	E-Field Polarization Relative to the Antenna and Aircraft	28
13a	Open Circuit Voltage for Vertical Case 1 Electric Field (200 nsec)	29
13b	Open Circuit Voltage for Vertical Case 1 Electric Field (1 μ sec)	29
14a	Open Circuit Voltage for Vertical Case 2 Electric Field (200 nsec)	30
14b	Open Circuit Voltage for Vertical Case 2 Electric Field (1 μ sec)	30
15a	Open Circuit Voltage for Horizontal Case 1 Electric Field (200 nsec)	31
15b	Open Circuit Voltage for Horizontal Case 1 Electric Field (1 μ sec)	31

LIST OF FIGURES (Continued)

<u>Figure</u>		<u>Page</u>
<u>Effect of Aircraft Response on Measurements (Con't)</u>		
16a	Open Circuit Voltage for Horizontal Case 2 Electric Field (200 nsec)	32
16b	Open Circuit Voltage for Horizontal Case 2 Electric Field (1 μ sec)	32
17a	Open Circuit Voltage for 30° Polarized Case 1 Electric Field (200 nsec)	34
17b	Open Circuit Voltage for 30° Polarized Case 1 Electric Field (1 μ sec)	34
18a	Open Circuit Voltage for 30° Polarized Case 2 Electric Field (200 nsec)	35
18b	Open Circuit Voltage for 30° Polarized Case 2 Electric Field (1 μ sec)	35
<u>Relationship Between Phase and Amplitude Under Causality Constraint</u>		
19	Contour of Integration in Complex ω Plane	41
20	Phase for a Constant Amplitude	48
21a	Amplitude Function	50
21b	Phase Function	50
22a	π Shift in Phase	51
22b	Amplitude for π Shift in Phase	51
<u>Difficulties in Using the Measured Effective Height Data</u>		
23	Orientation for Free Field Relative to the C-130 Model Aircraft	56
24	Scaled Frequency Bands	57
25	Effective Length Amplitude	59
26a	Effective Length Phase Horizontal Polarization (Preliminary)	60
26b	Effective Length Phase Horizontal Polarization (Final)	60
27a	Effective Length Phase Vertical Polarization (Preliminary)	61

LIST OF FIGURES (Continued)

<u>Figure</u>		<u>Page</u>
<u>Difficulties in Using the Measured Effective Height Data</u>		
27b	Effective Length Phase Vertical Polarization (Final)	61
28a	Effective Length 45 Degree Polarization (Preliminary)	62
28b	Effective Length 45 Degree Polarization (Final) . . .	62
29	Vertical Polarization $h_e(t)$	64
30a	V_{oc} for Measured Effective Height (Vertical Polarization)	65
30b	V_{oc} for Measured Amplitude and Calculated Phase (Vertical Polarization)	65
31	Horizontal Polarization $h_e(t)$	66
32a	V_{oc} for Measured Effective Height (Horizontal Polarization)	68
32b	V_{oc} for Measured Amplitude and Calculated Phase (Horizontal Polarization)	68
33a	45° Polarization Calculated Amplitude (10 MHz) . . .	69
33b	45° Polarization Calculated Amplitude (100MHz) . . .	69
34a	45° Polarization Calculated Phase	70
34b	45° Polarization Calculated Phase	70
<u>Effective Heights for Antennae on Conducting Surfaces</u>		
35	Dipole and Monpole Over Ground Plane	77
36	Incident Field on a Monopole Antenna	78
37	Incident Field on an Antenna Mounted on Cylinder . .	78
38	Electrostatic Field from a Finite Cylinder in a Vertical Field	80
39	Electrostatic Field from a Finite Cylinder in a Horizontal Field	80

SECTION I
INTRODUCTION

For a number of years, people have been concerned about the accuracy of electric field measurements made from antennas on aircraft. This concern has primarily been directed at the distortions in the field at the antenna caused by the presence of the aircraft.

In 1975, the Boeing Company under contract with the Defense Nuclear Agency (DNA) measured the complex effective height (h_e) for a one meter blade antenna on a C-130 aircraft. The experimental procedures and estimates of the accuracy of these measurements are discussed in Reference 1 and will not be repeated here except to the extent necessary to indicate certain difficulties in using that data.

The purpose of these measurements was to ascertain the effect of the C-130 aircraft response on free field electromagnetic field measurements. Knowing the antenna effective height ($h_e(\omega)$) and the transfer function for the antenna delay line and oscilloscope circuit ($T(\omega)$), one can relate the scope voltage ($V_s(\omega)$) to the free space electric field in the frequency domain ($E(\omega)$) by the formula

$$V_s(\omega) = T(\omega) \cdot h_e(\omega) \cdot E(\omega). \quad (1)$$

A complexity is added when one considers the polarization of the electric field; however, using the principle of superposition, one can handle polarization effects in the plane perpendicular to the direction of propagation of the incident field. For this reason both the vertical (E aligned along the antenna axis) and the horizontal (E aligned along the fuselage axis) effective heights were measured. Thus for an incident field (E)-polarized at an angle α with respect to the antenna axis, Eq. 1 becomes

$$V_s(\omega) = T(\omega) \cdot [h_e(\omega)_v \cdot \cos \alpha + h_e(\omega)_h \cdot \sin \alpha] \cdot E(\omega). \quad (2)$$

To represent the effect of these transfer functions in the time domain, the procedure is as follows: First, the free field is transformed to the frequency domain by

$$E(\omega) = \int_0^{\infty} dt e^{i\omega t} E(t). \quad (3)$$

Then, Eq. 2 is used and the inverse Fourier transform of $V_s(\omega)$ is taken as shown in Eq. 4:

$$V_s(t) = \int_{-\infty}^{\infty} \frac{d\omega}{2\pi} \cdot T(\omega) \cdot [h_e(\omega)_v \cdot \cos \alpha + h_e(\omega)_h \cdot \sin \alpha] \cdot E(\omega) \cdot e^{-i\omega t}. \quad (4)$$

In this report, the transfer function for the antenna and equipment was assumed to be unity, and just the effect of the aircraft response investigated, utilizing Eq. 4. While implementing this equation seems straightforward, difficulties were encountered because the effective heights reported in Reference 1 were non-causal. These difficulties are discussed in Section II along with calculated phase functions for the effective heights that do preserve causality. In Section III, effective height functions utilizing the Boeing amplitude data and calculated phases were used to show the effect of the aircraft response on vertical, horizontal and 30° polarized incident fields. Conclusions are drawn in Section IV about the quality of electric field measurements made using the C-130 aircraft antenna. Additional discussions concerning the theory of amplitude and phase relationships, the difficulties with the measured effective heights and the complexity of estimating effective heights for antennas on ground planes are contained in the appendices.

SECTION II

AIRCRAFT RESPONSE TRANSFER FUNCTIONS

In the Boeing measurement program [1] both the amplitude and phase of the complex antenna effective height were measured. The estimated errors associated with these measurements were $\pm 2\text{dB}^*$ for the amplitude and $\pm 30^\circ$ for the phase. However, there was an additional ambiguity associated with the data reduction of the phase which allowed any phase points to differ by $\pm 180^\circ$ and any of the scaled frequency regions to differ by $\pm 90^\circ$ [2]. It was due to this ambiguity that phase data were revised between the preliminary draft [3] and the final report [1] to provide correlation between the vertical, horizontal and 45° data. (See Appendix B.)

The major difficulty with using the effective heights reported is that they appear to be non-causal. This non-causal result is primarily attributed to inaccuracies in the phase.

As an example of the problems associated with using a non-causal effective height, consider Eq. 4 where $T(\omega) = 1$ and $\alpha = 0^\circ$. Then,

$$v_s(t) = \int_{-\infty}^{\infty} \frac{d\omega}{2\pi} e^{-i\omega t} h_e(\omega) \cdot E(\omega). \quad (5)$$

Equation 5 can be reduced to a convolution integral with

$$v_s(t) = \int_0^{\infty} dt' \cdot E(t') \cdot h_e(t-t') \quad (6)$$

where $E(t) = 0$ for $t < 0$.

Now, if $h_e(t)$ is causal, then $h_e(t) = 0$ when $t < 0$, so the upper limit on Eq. 6 would be t . However, if $h_e(t) \neq 0$ when $t < 0$,
* dB error is defined as $\text{dB} = 20 \log_{10} \frac{(A+\epsilon)}{A}$.

- [1] Antenna Effective Length Measurement, The Boeing Company, Seattle, Washington, DNA 3798F-1,2, July 1975.
- [2] Letter from D. D. Connell (Boeing) to Major W. Adams, DNA dated 23 September 1975.
- [3] Antenna Effective Length Measurement, The Boeing Company, Seattle, Washington, D180-18878-1,2, July 1975 (draft).

then there are contributions to $V_s(t)$ from the integration of $t' > t$ or an error is introduced of the order

$$\epsilon(V_s) = \int_t^\infty dt' \cdot E(t') \cdot h_e(t-t'). \quad (7)$$

Physically, this means that the antenna is responding before the field has arrived which is impossible. Figure 1 shows the function $h_e(t)$ as computed from the Boeing data for the vertical and horizontal data, and one can note the extent of the precursor for $t < 0$. The procedure for calculating $h_e(t)$ is explained in Appendix B. To correct this deficiency, one could force the function $h_e(t)$ to zero at $t = 0$ and use a convolution integral. However, aside from the practical problem of needing to perform N^2 calculations for a waveform out to $t = N \cdot \Delta t$, there is the more important question of the accuracy of such a forced calculation.

A more reasonable solution to this problem has been found by assuming that the amplitude data is accurate to within the estimated errors and then calculating a causal phase function. The theory for relating amplitude and phase in a causal manner is discussed in Appendix A. The results of these phase calculations are given in the following subsections for both the vertical and horizontal polarizations.

2.1 VERTICAL EFFECTIVE HEIGHT

The amplitude data for the vertical effective height is shown in Figure 2. The data was taken over the frequency range from 0.5 MHz to 100 MHz with the dashed lines indicating the extrapolations used to calculate the phase. This data shows that the low frequency effective height is approximately half the physical height as opposed to a value equal to the physical height which one would expect for an antenna over a conducting ground plane.* This decrease for an expected value of 1 m can be qualitatively explained by the simple models shown in Appendix C.

* In discussing effective heights of antennas over a ground plane one must distinguish between the ratio of open circuit voltage to free field versus open circuit voltage to free field plus reflected field. For our effective heights we assumed the former.

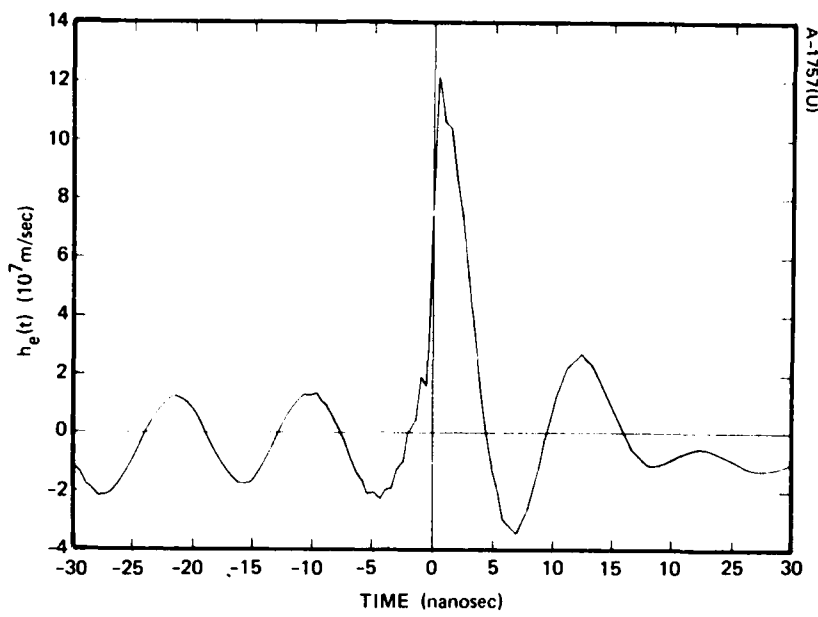


Figure 1a. $h_e(t)$ for the Vertically Polarized Data

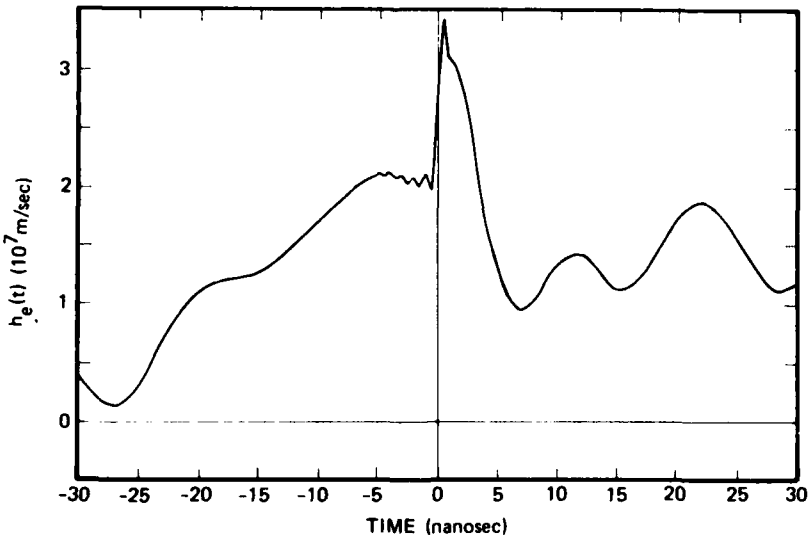


Figure 1b. $h_e(t)$ for the Horizontally Polarized Data

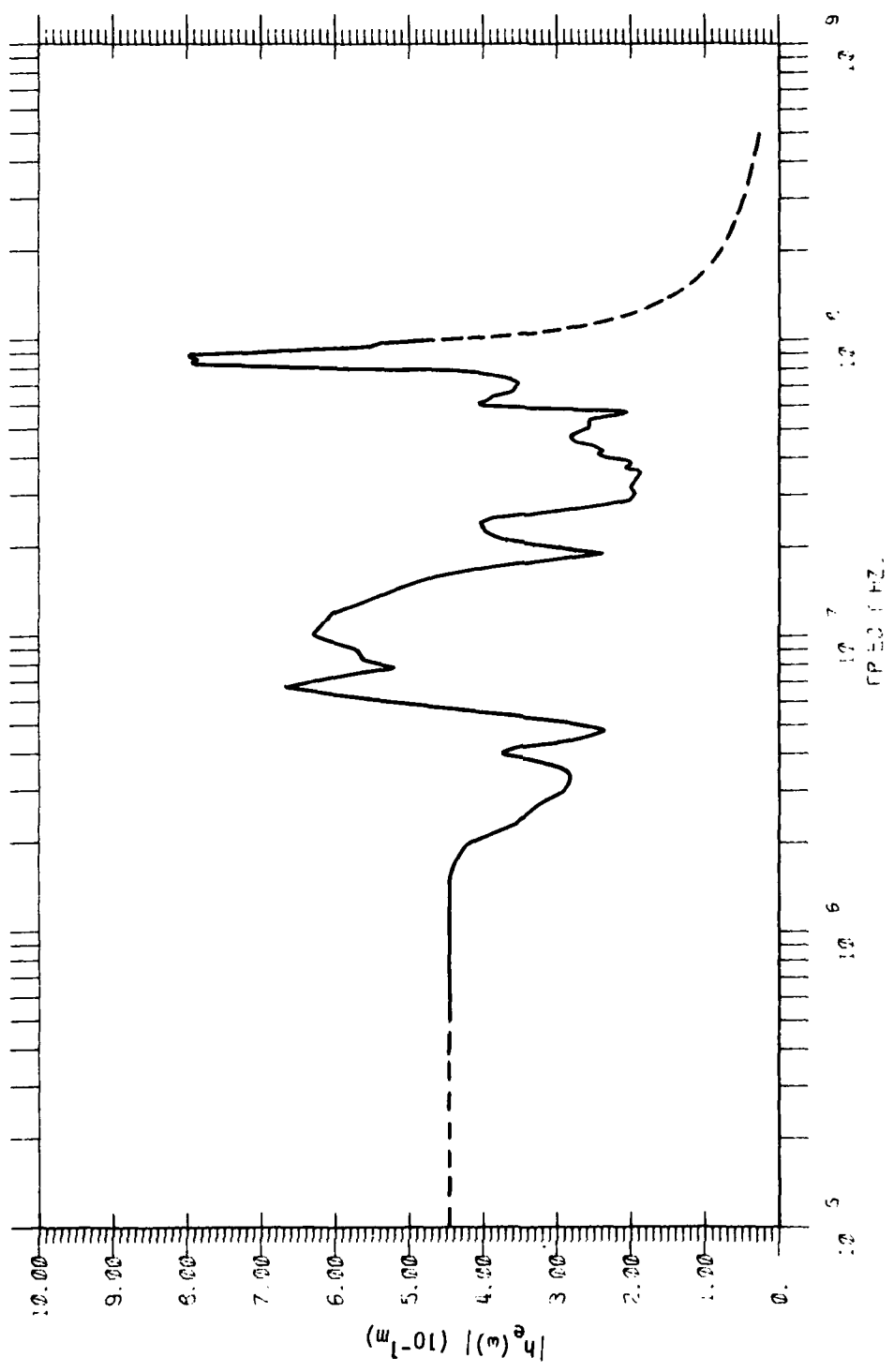


Figure 2. $|h_e(\omega)|$ for Vertical Electric Field

Using this amplitude data, one can calculate a causal phase function from the formula derived in Appendix A. Namely,

$$\phi(\omega) = \phi_{\infty}(\omega) - \frac{2\omega}{\pi} \int_0^{\infty} \frac{dz}{(z^2 - \omega^2)} \ln[A(z)/A_{\infty}(z)] - \ln[A(\omega)/A_{\infty}(\omega)]. \quad (8)$$

In order to use this equation we need to know how the amplitude data extrapolates to both $\omega = 0$ and $\omega = \infty$ and also what the phase value is for large ω .

For low frequencies, the effective height of a monopole antenna on a conducting surface goes to a constant value, as discussed in Appendix C. Thus, for $\omega < 2\pi \cdot (0.5 \text{ MHz})$

$$A(\omega) = A[2\pi \cdot (0.5 \text{ MHz})]. \quad (9)$$

For the high frequencies, we know that a dipole effective height falls off like $1/\omega$ and that a monopole over a ground plane is electrically/equivalent to a center fed dipole. Thus, we want our extrapolated function to have a $1/\omega$ dependence at very high frequencies. In addition, we want it to have a smooth transition from the measured data. As can be seen in Figure 2, there appears to be a resonance in the amplitude data at 85 MHz. This resonance can be fit by the form

$$A(\omega) = \frac{(0.8) \cdot \omega \cdot \Delta\omega}{[(\omega_0 - \omega^2)^2 + (\omega\Delta\omega)^2]^{1/2}} \quad (10)$$

where $\omega_0 = 2\pi \cdot (85 \text{ MHz})$

$\Delta\omega = 2\pi \cdot (85 \text{ MHz})$.

We note that for $\omega \gg \omega_0$, $A(\omega) \rightarrow 1_0/\omega$. Therefore, for $\omega > 2\pi \cdot (100 \text{ MHz})$ the amplitude was extrapolated using Eq. 10.

For a function whose amplitude decays as $1/\omega$, the phase changes by $\pi/2$ during that fall off (see Appendix A); thus, the phase infinity (ϕ_{∞}) is $\pi/2$.

These are the parameters and functions which were used to calculate the vertical phase function. It should be noted that the purpose of these extrapolations beyond the frequency band measured (.5 to 100 MHz) was not to gain information outside that band, but

rather to insure that we do not introduce non-physical, erroneous features in the applicable time transformed data.

The calculated phase function is shown in Figure 3. For comparison purposes, the measured phase data have also been plotted. One can note that other than the 180° phase shift at the beginning of the data the curves are in fair agreement, particularly when one considers the $\pm 90^\circ$ ambiguity on the measured data. Figure 4 and 5 show the delta and step function responses for the combined measured amplitude and calculated phase curves. As is shown in Appendix B, the complex effective height for the vertical polarization described by the amplitude data (Figure 2) and the calculated phase function (Figure 3) is now causal in the time domain.

2.2 HORIZONTAL EFFECTIVE HEIGHT

The amplitude data for the horizontal effective height is shown in Figure 6. Again, the dashed lines represent the extrapolations used to calculate the phase. For this data we note that the effective height is equal to the physical height at the low frequencies. A simple model for the coupling of a horizontal field with a vertical antenna is shown in Appendix C and basically involves the coupling of the dipole field generated by the fuselage with the antenna. An important point to note is that the coupled voltage will change sign depending on which way the incident free field is polarized.

Using Equation 8 we have calculated a causal phase function. In performing this calculation we have used the following extrapolations for the amplitude data. For low frequencies, we again have a constant value which reflects the fairly constant charge distribution on the fuselage for frequencies below the fuselage resonance of ~ 2 MHz.

Therefore, for $\omega < 2\pi \cdot 0.5$ MHz)

$$A(\omega) = A(2\pi \cdot 0.5 \text{ MHz}) . \quad (11)$$

For high frequencies, we again note that the data shown in Figure 6 has a $1/\omega$ decay, which is consistent with a dipole created by the fuselage. Therefore, for frequencies above $(2\pi \cdot 100$ MHz) we used the form

$$A(\omega) = \left[A(2\pi \cdot 100 \text{ MHz}) - \frac{\omega_0}{\omega_1} \right] \left(\frac{\omega_1}{\omega} \right)^{\omega} + \frac{\omega_0}{\omega} \quad (12)$$

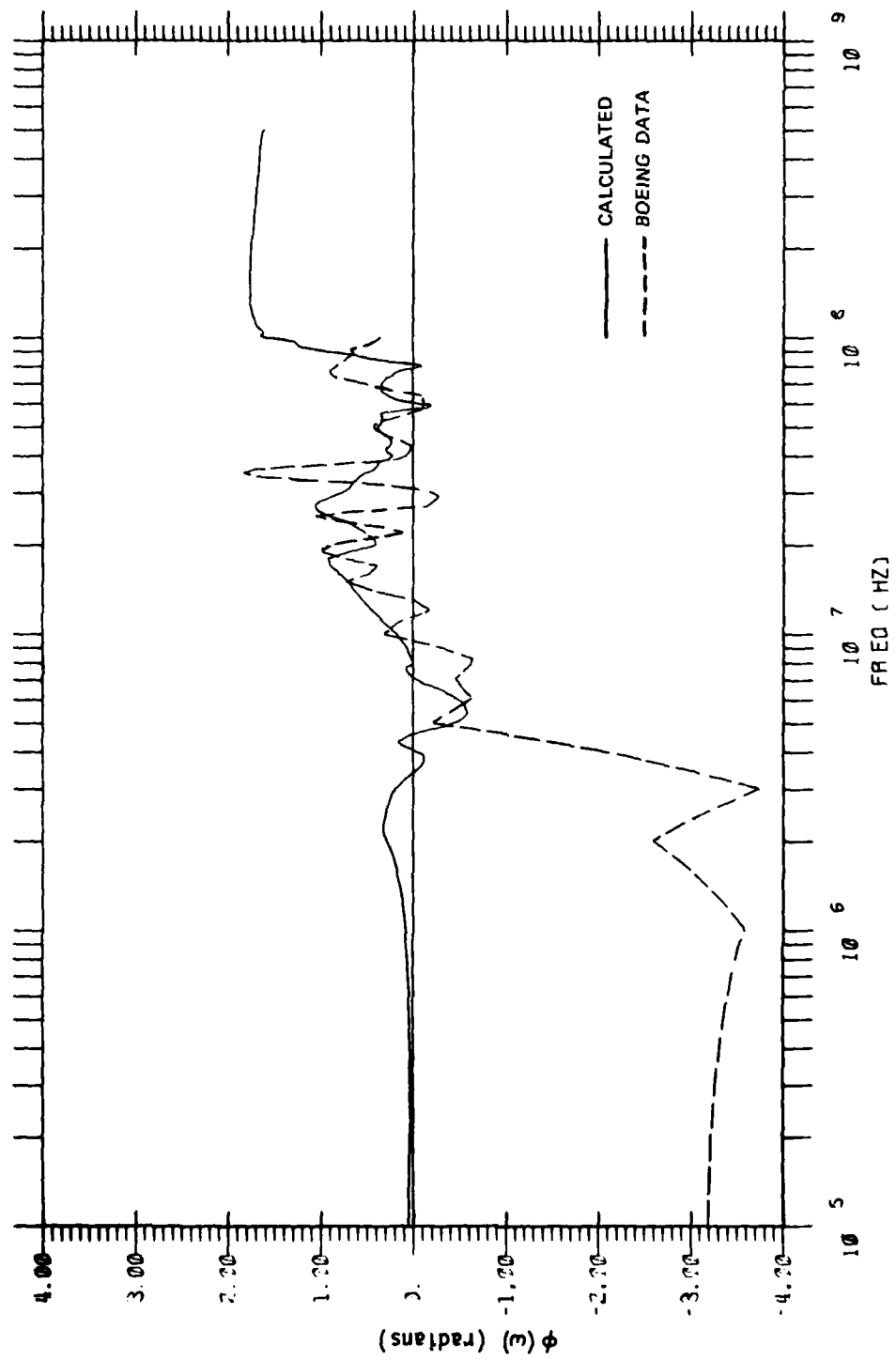


Figure 3. Phase of $h_e(\omega)$ for a Vertical Electric Field

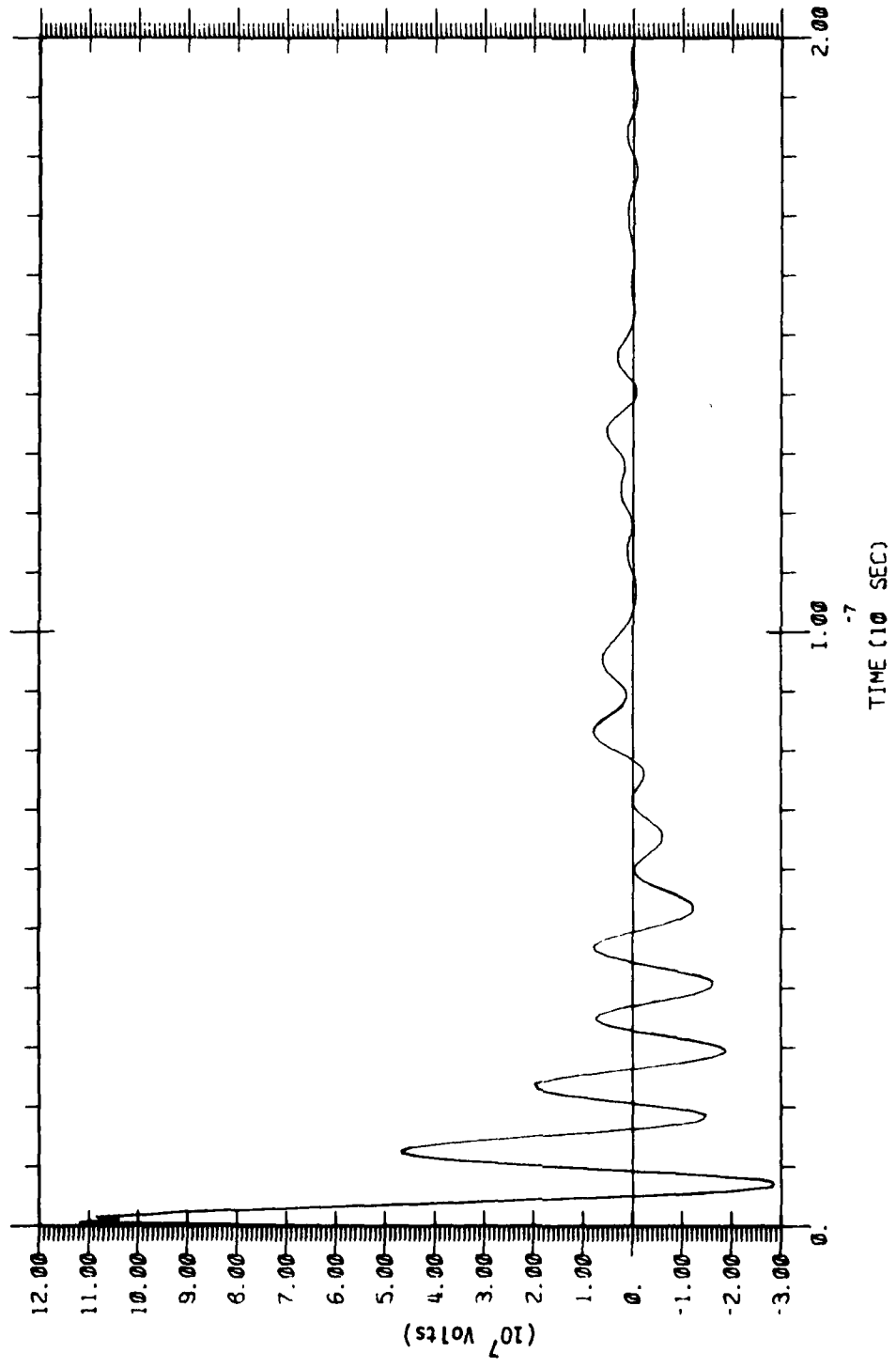


Figure 4. Delta Function Response for Vertical Polarization

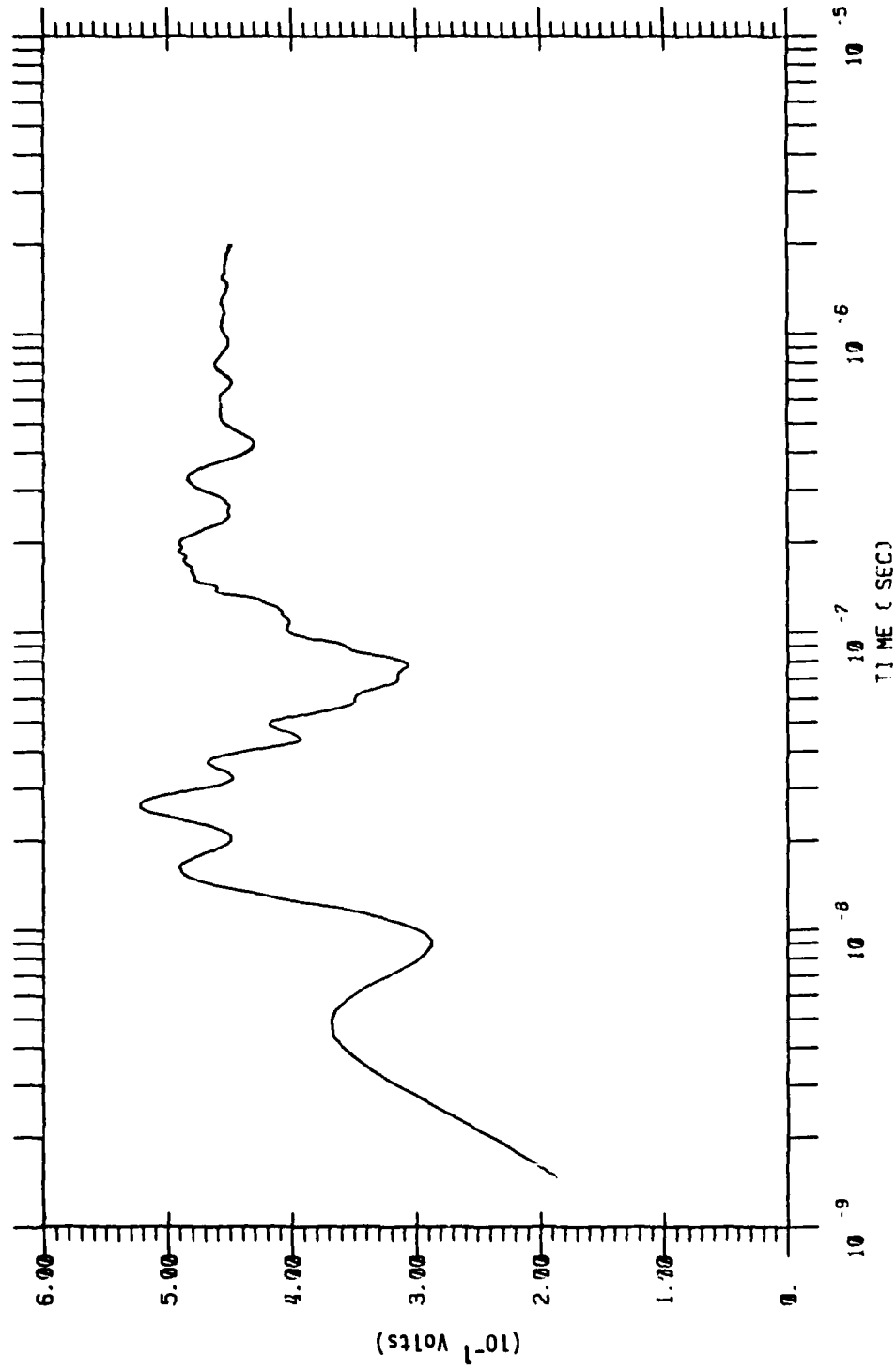


Figure 5. Step Function Response for Vertical Polarization

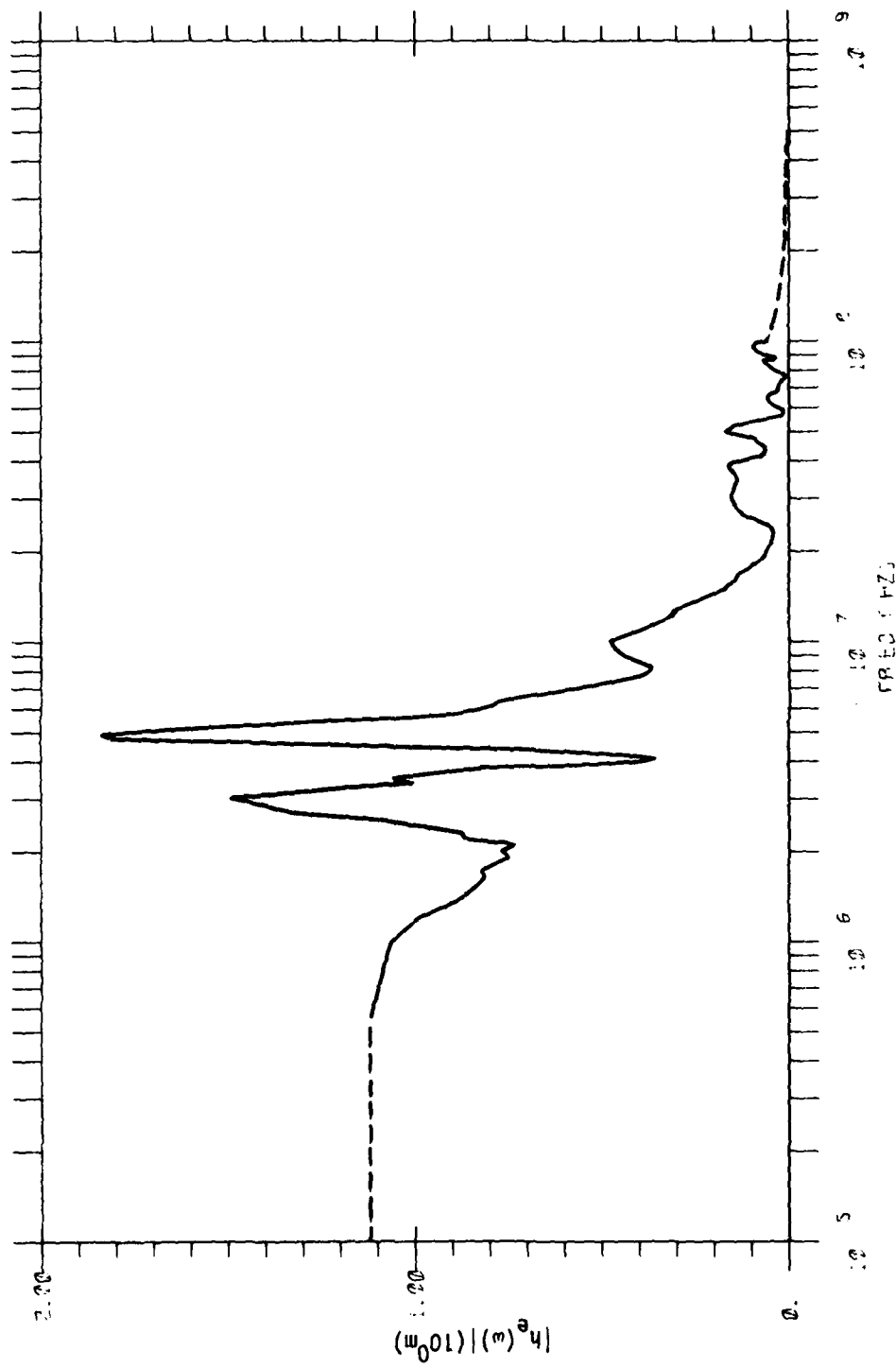


Figure 6. $|h_e(\omega)|$ for a Horizontal Electric Field

where $\omega_0 = 2 \text{ MHz} \cdot 2\pi$
 $\omega_1 = 100 \text{ MHz} \cdot 2\pi$.

The first term in Eq. 12 provides a transition for the data to the high frequency form. Again, for a $1/\omega$ decay the phase changes by $\pi/2$, so $\phi_\infty = \pi/2$.

Figure 7 shows the calculated phase along with the measured phase data. At first glance there appears to be considerable difference; however, it should be noted that given the $\pm 30^\circ$ accuracy of the data and the $\pm 90^\circ$ ambiguity within scaled frequency bands (see Appendix B) the difference may not be as great. Figures 8 and 9 are graphs of the delta and step function response using the amplitude data and the calculated phase function.

As a further check on the accuracy of these new effective height functions, they have been used to predict the effective height for a 45° polarization and then compared with the measured data for 45° . This comparison is discussed in Appendix B.

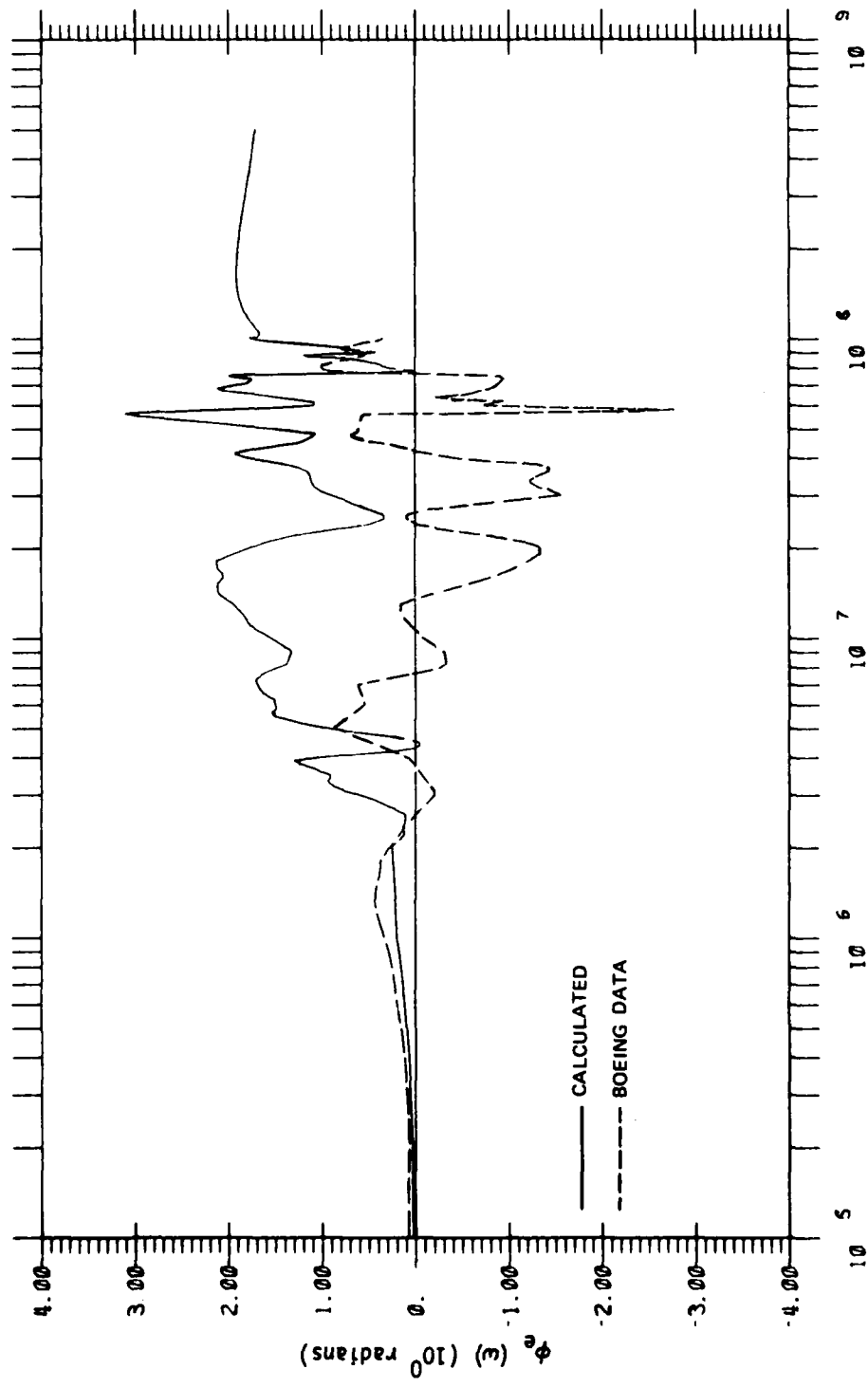


Figure 7. Phase of $h_e(\omega)$ for a Horizontal Electric Field

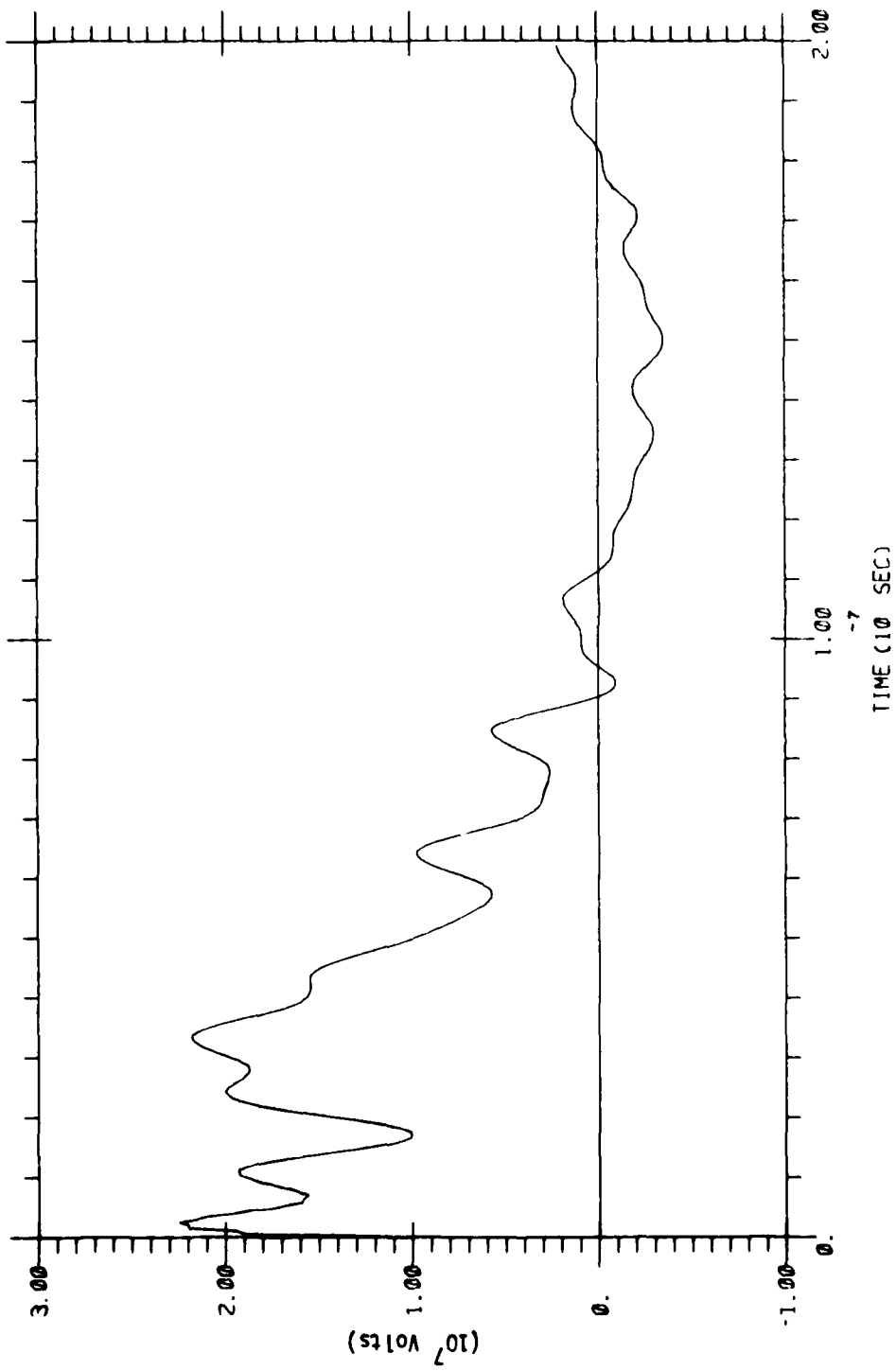


Figure 8. Delta Function Response for Horizontal Polarization

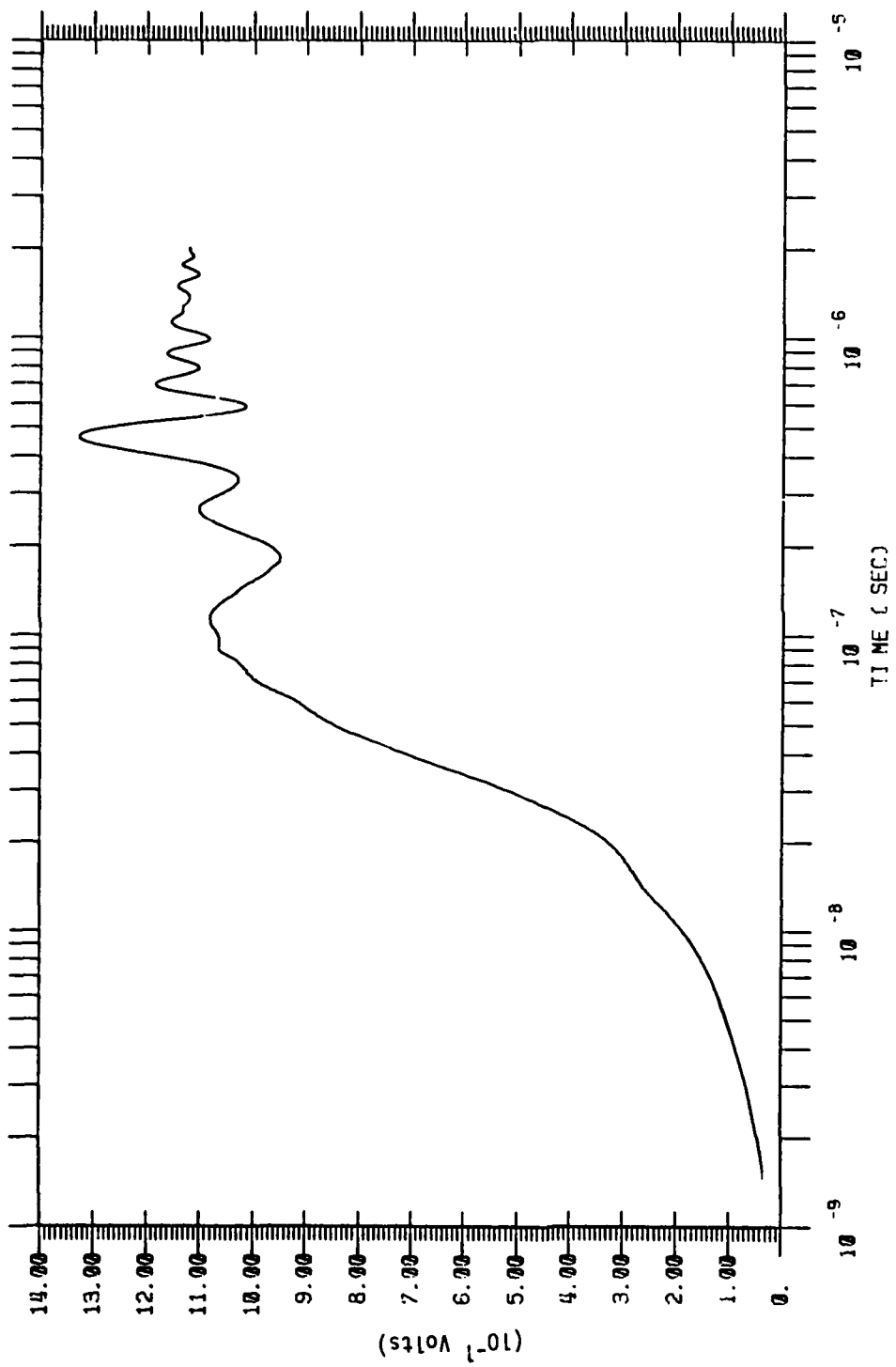


Figure 9. Step Function Response for Horizontal Polarization

SECTION III.

EFFECT OF AIRCRAFT RESPONSE ON MEASUREMENTS

The effective height functions which were discussed in Section II can be used to investigate the sensitivity of electric field measurements made on such an aircraft platform. For the free field, we have assumed an analytic function of the form

$$E(t) = E_0 \frac{e^{a(t-T)}}{1 + e^{b(t-T)}} . \quad (13)$$

The Fourier transform of such a function is

$$E(\omega) = \frac{E_0 \pi}{b} \left\{ \frac{e^{i\omega T}}{\sin \left[\frac{\pi}{b}(a+i\omega) \right]} \right\} . \quad (14)$$

The amplitude and phase are given by the following equations.

$$|E(\omega)| = E_0 \frac{\sqrt{2\pi}}{b} \left[\cosh(2A) - \cos(2B) \right]^{-1/2} \quad (15)$$

and

$$\phi_E(\omega) = \omega T + \tan^{-1} \left[-\frac{\tanh(A)}{\tan(B)} \right] \quad (16)$$

$$\text{where } A = \frac{\pi\omega}{b} \\ B = \frac{\pi a}{b} .$$

Figures 10 and 11 show the time waveform and its Fourier transform for two sets of parameters, with the peak value normalized to one.

$$\begin{aligned} \text{Case 1)} \quad & a = 2.0 \times 10^8 \\ & b = 2.7 \times 10^8 \\ & T = 5.0 \times 10^{-8} \end{aligned}$$

$$\begin{aligned} \text{Case 2)} \quad & a = 2.0 \times 10^8 \\ & b = 2.1 \times 10^8 \\ & T = 5.0 \times 10^{-8} \end{aligned}$$

Using the above analytic form with both sets of parameters, we have calculated the equivalent open circuit voltage at the antenna

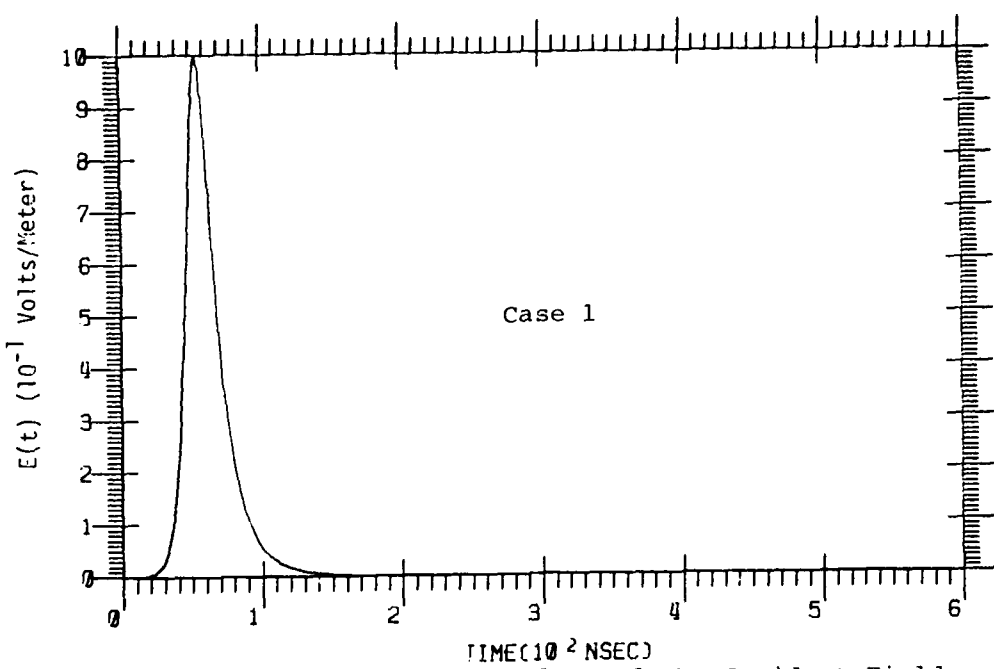


Figure 10a. Time Waveform of the Incident Field

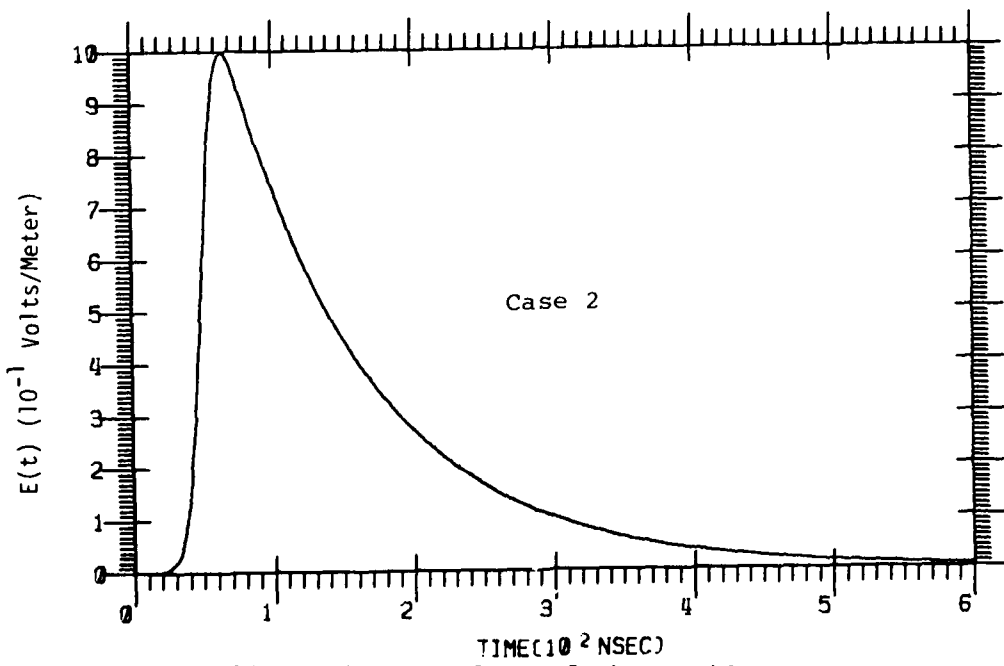


Figure 10b. Time Waveform of the Incident Electric Field

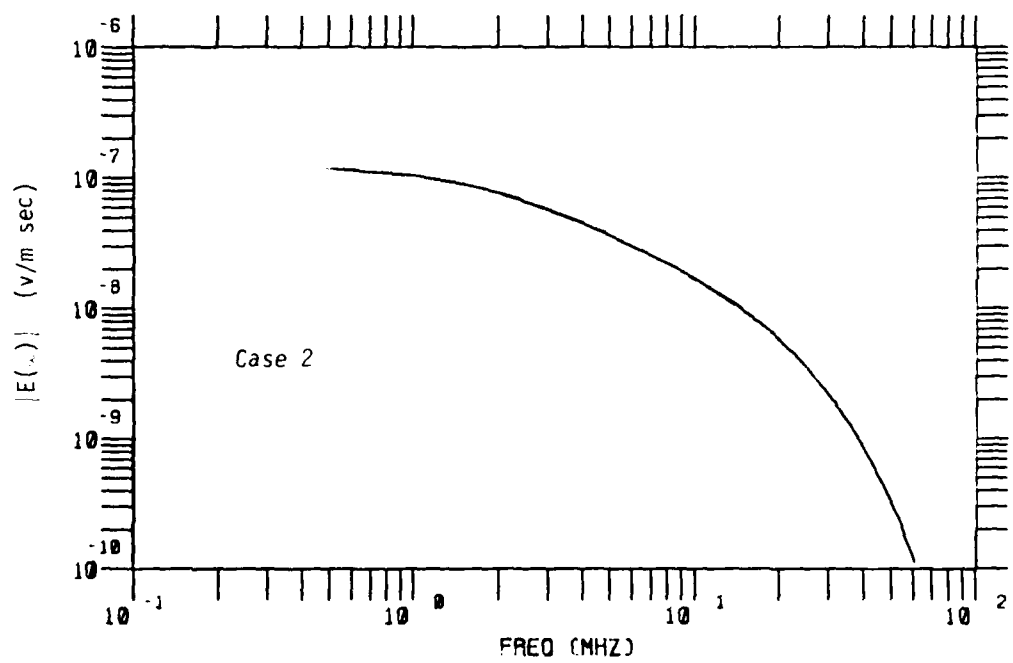
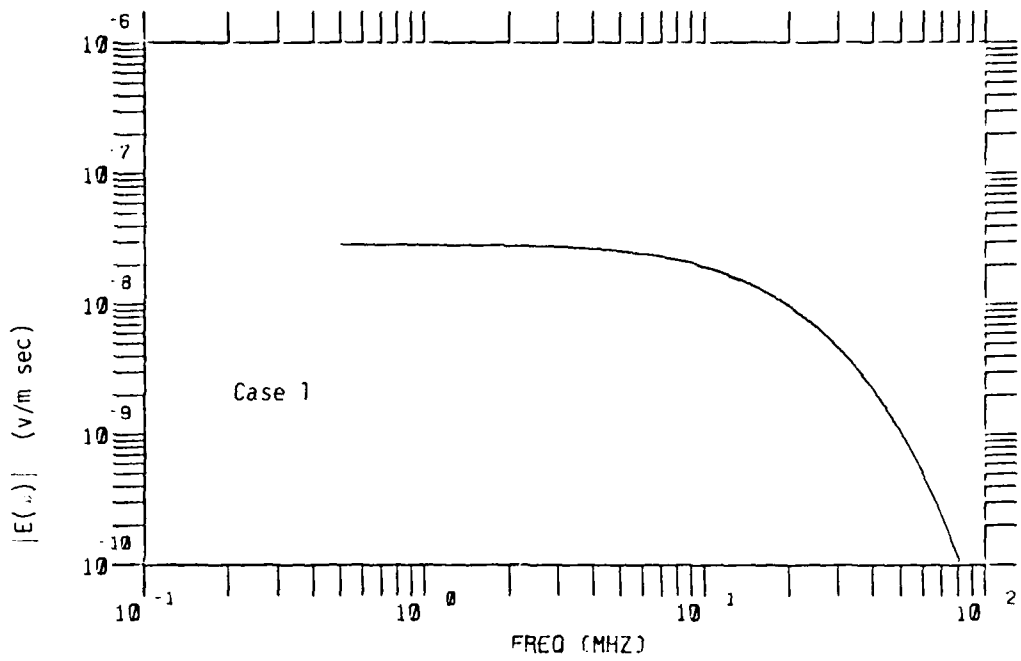


Figure 11a. $|E(.,.)|$ for the Incident Electric Fields

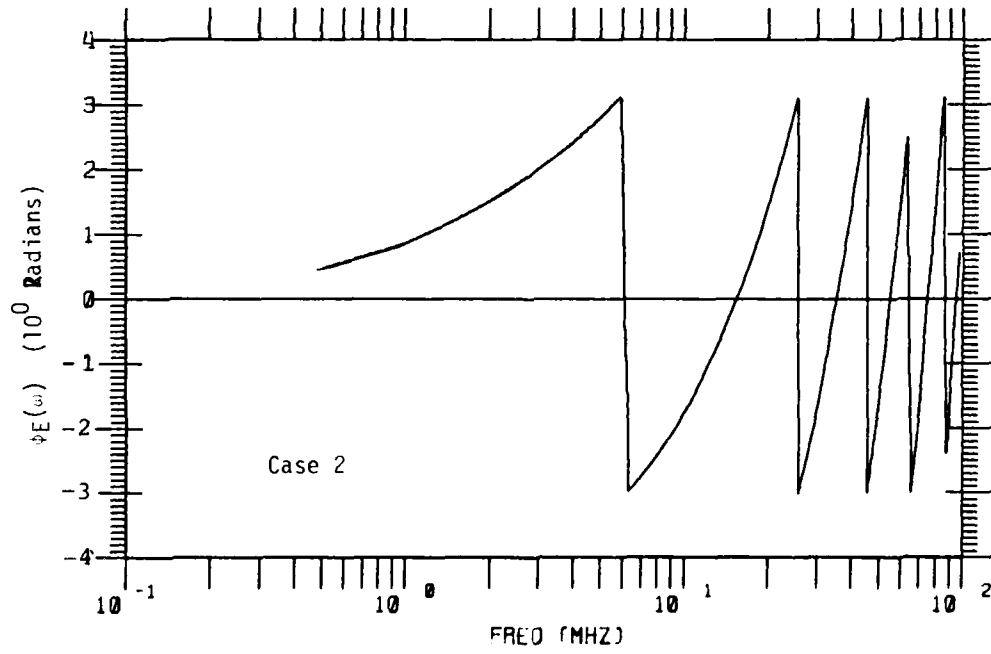
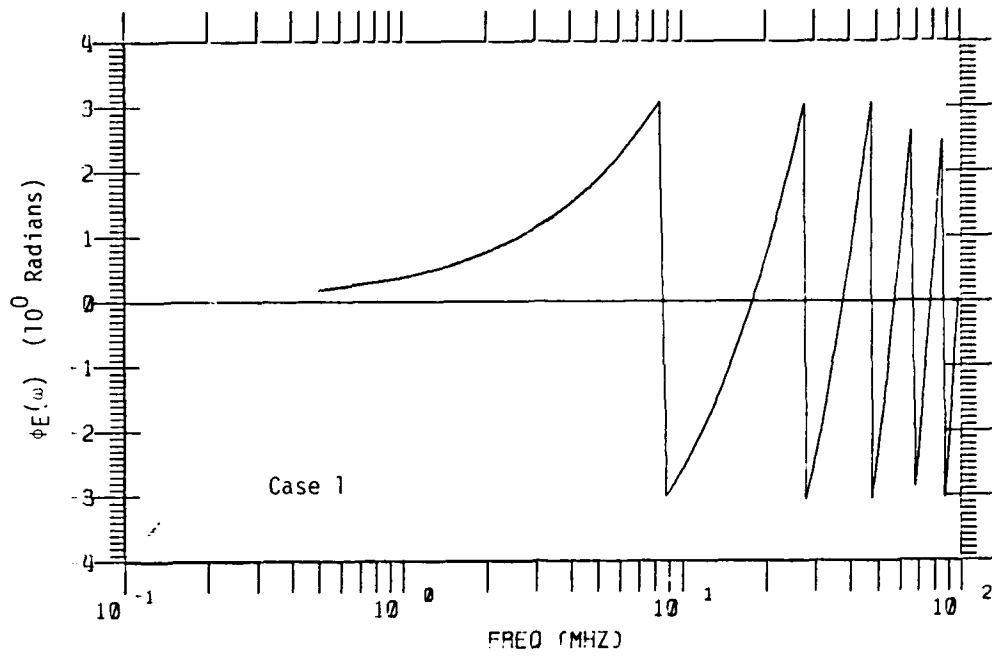


Figure 11b. Phase for the Incident Electric Fields

Eq. 1, for three electric field polarizations: (1) vertical, the E-field aligned along the antenna (2) horizontal, the E-field aligned along the fuselage, and (3) 30° , the E-field aligned at 30° with respect to the antenna and pointing toward the front of the aircraft. Figure 12 shows the orientation for each polarization.

3.1 VERTICAL POLARIZATION EFFECTS

The antenna open circuit voltage as a function of time for a case 1 vertical field is shown in Figure 13. Also overlaid on the graph is the voltage waveform that would have resulted if the effective height had been constant and equal to the physical height (1 m). We will refer to this waveform as the "free field voltage". This reduction in peak voltage below the one-half value expected from the low frequency effective height data is caused by the narrowness (high frequency nature) of the incident pulse. Figure 14a and 14b show similar calculations for the slower decaying pulse (lower frequency) of case 2. For this case the peak voltage is approximately 0.5 as expected. In both cases there is a rippling in the calculated voltage caused by the resonances in the effective height data at approximately 5 to 10 MHz.

3.2 HORIZONTAL POLARIZATION EFFECTS

For an incident electric field that is horizontally polarized there is still a voltage generated on the antenna. Figures 15a and 15b show the calculated antenna open circuit voltage for an incident field with case 1 parameters. Also shown in this graph for reference is the voltage that would be on the antenna if the field had been vertical and the effective height equal to the physical height (1 m). Note, for this polarization, the shape of the antenna voltage is much slower than the "free field voltage". For the slower decaying incident field of case 2 (Figures 16a and 16b), we note that the peak of the antenna voltage is significantly increased due to the larger low frequency content in the incident free field. In both cases we see there are oscillations caused by aircraft resonances. These calculations show that for an antenna mounted near the front of the fuselage there can be a strong contaminant signal on a vertical antenna from a horizontally polarized free field. This cross-polarized coupling is caused by the E field generated by charge distributions induced on the aircraft, notably the fuselage, and is basically a low frequency effect as shown in Appendix C. The effect of this cross coupling will

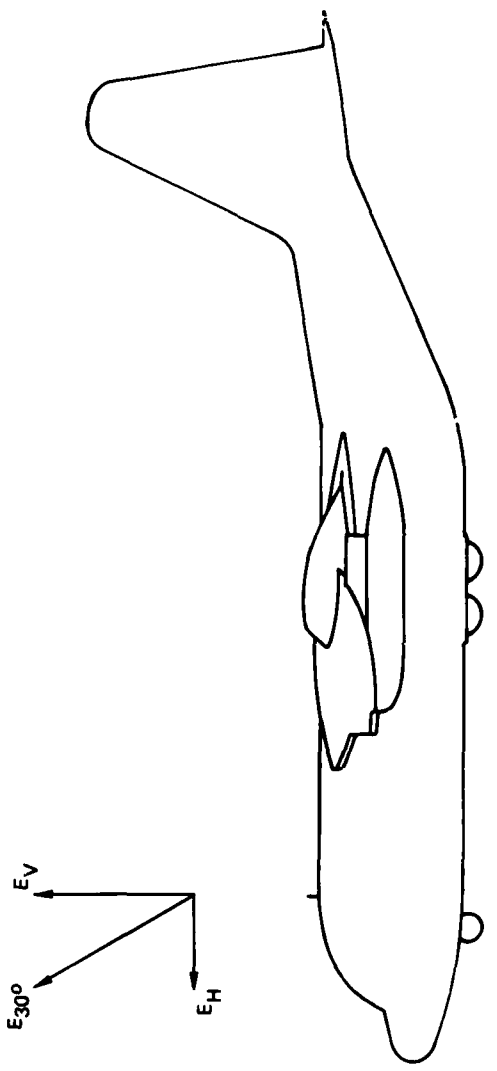


Figure 12. E-field Polarization Relative to the Antenna and Aircraft

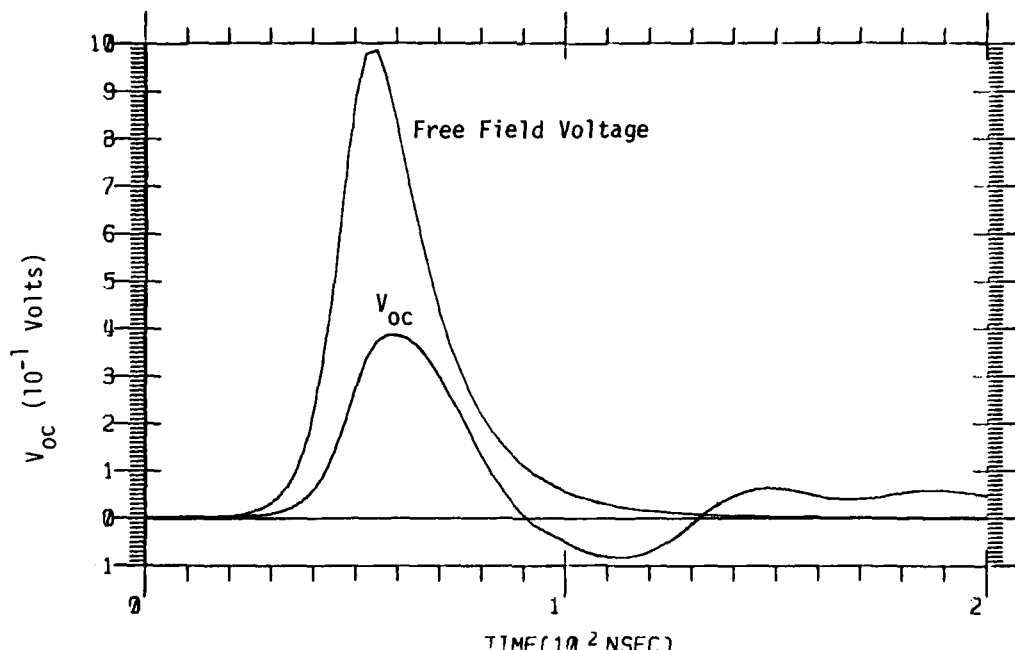


Figure 13a. Open Circuit Voltage for Vertical Case 1
Electric Field (200 nsec)

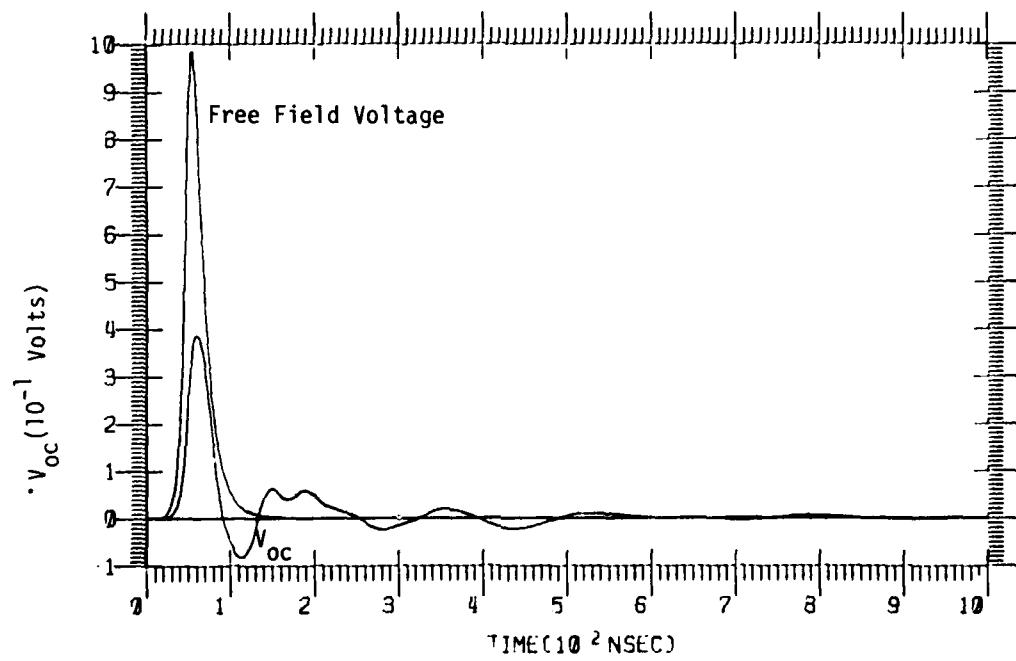


Figure 13b. Open Circuit Voltage for Vertical Case 2
Electric Field (1 μ sec)

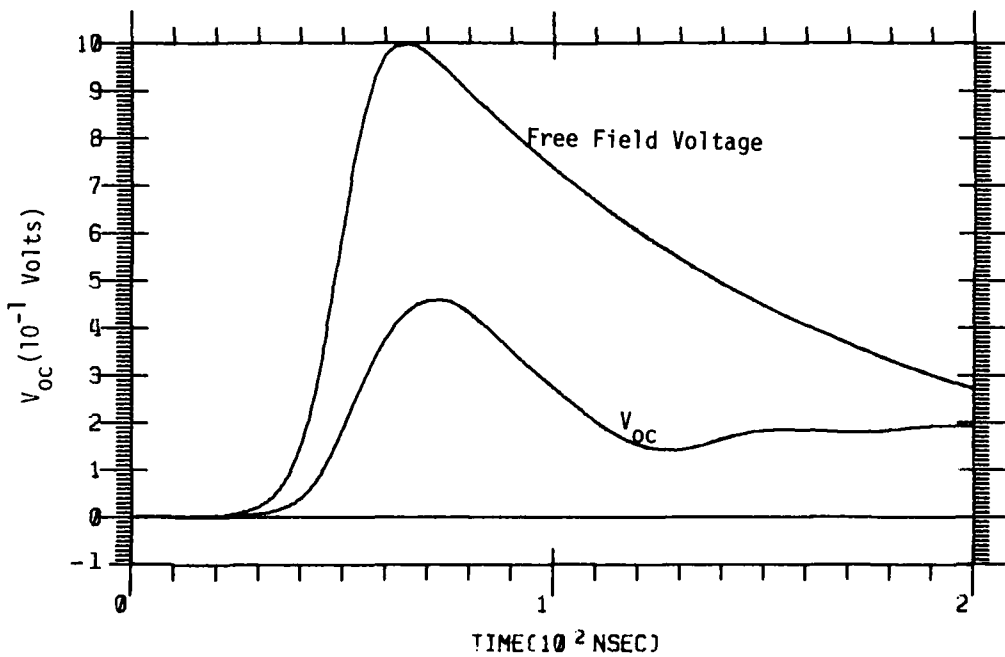


Figure 14a. Open Circuit Voltage for Vertical Case 2
Electric Field (200 nsec)

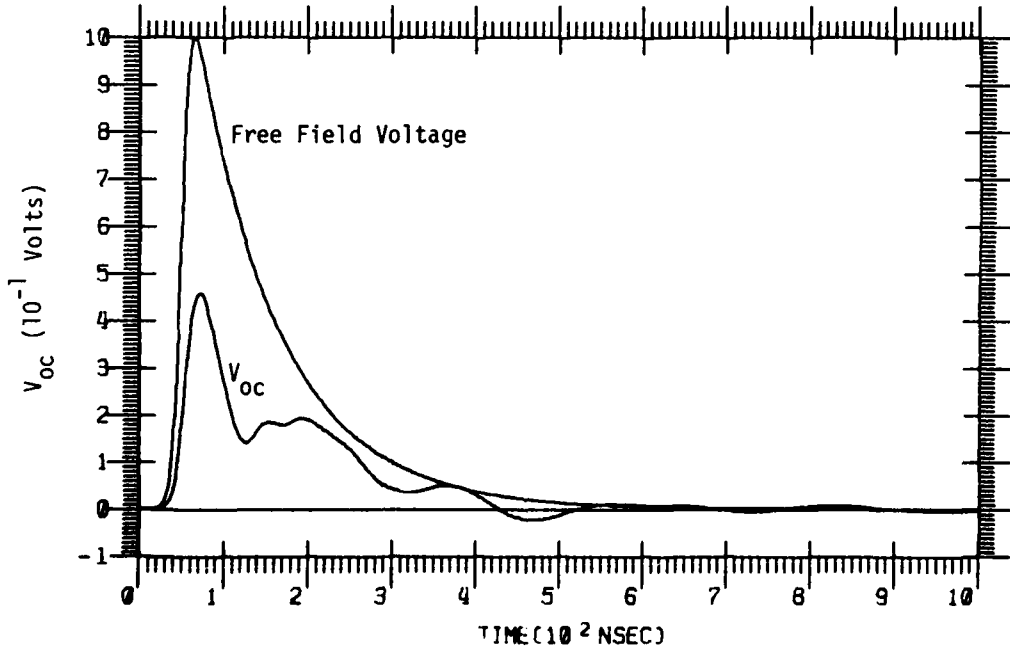


Figure 14b. Open Circuit Voltage for Vertical Case 2
Electric Field (1 μ sec)

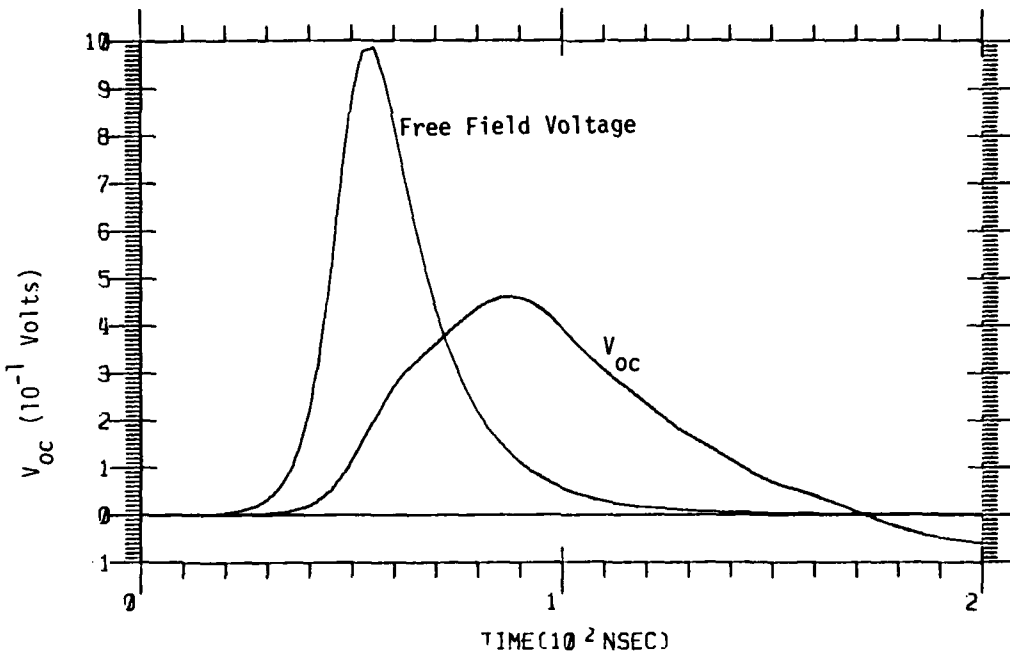


Figure 15a. Open Circuit Voltage for Horizontal Case 1
Electric Field (200 nsec)

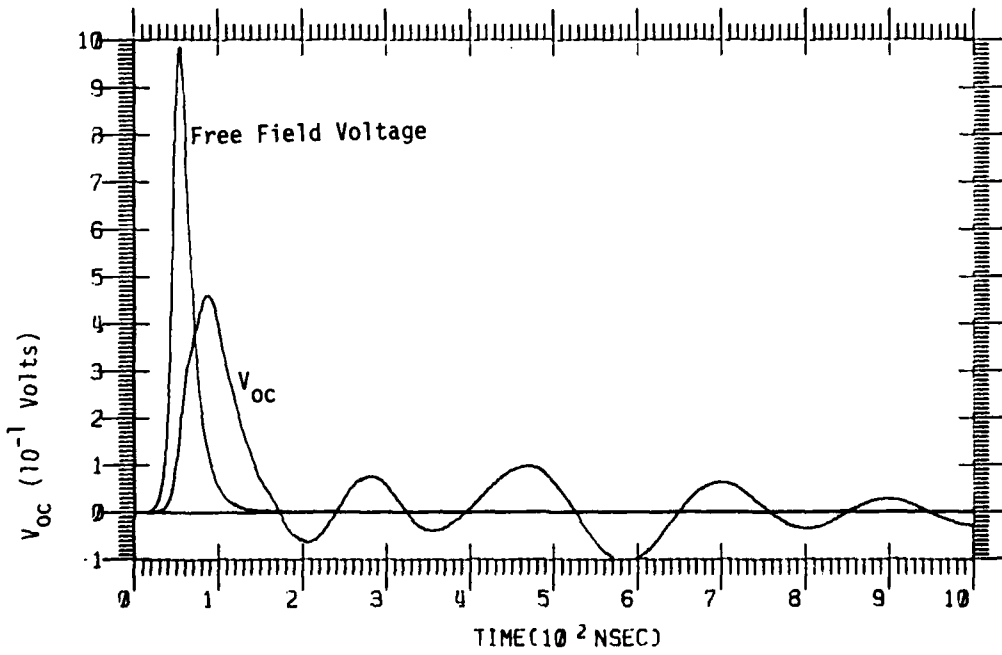


Figure 15b. Open Circuit Voltage for Horizontal Case 1
Electric Field (1 μ sec)

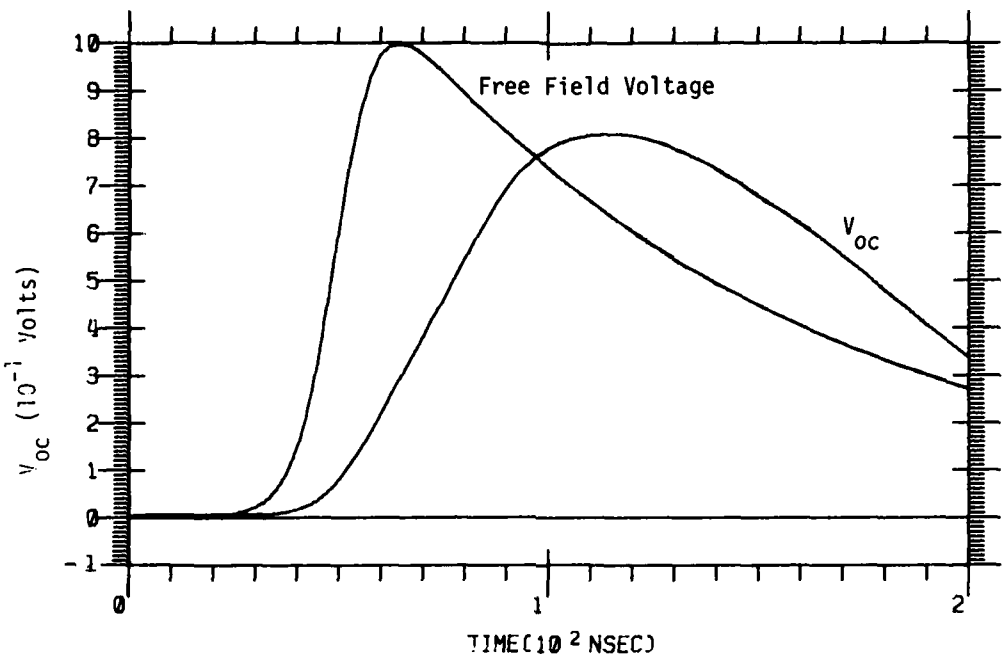


Figure 16a. Open Circuit Voltage for Horizontal Case 2
Electric Field (200 nsec)

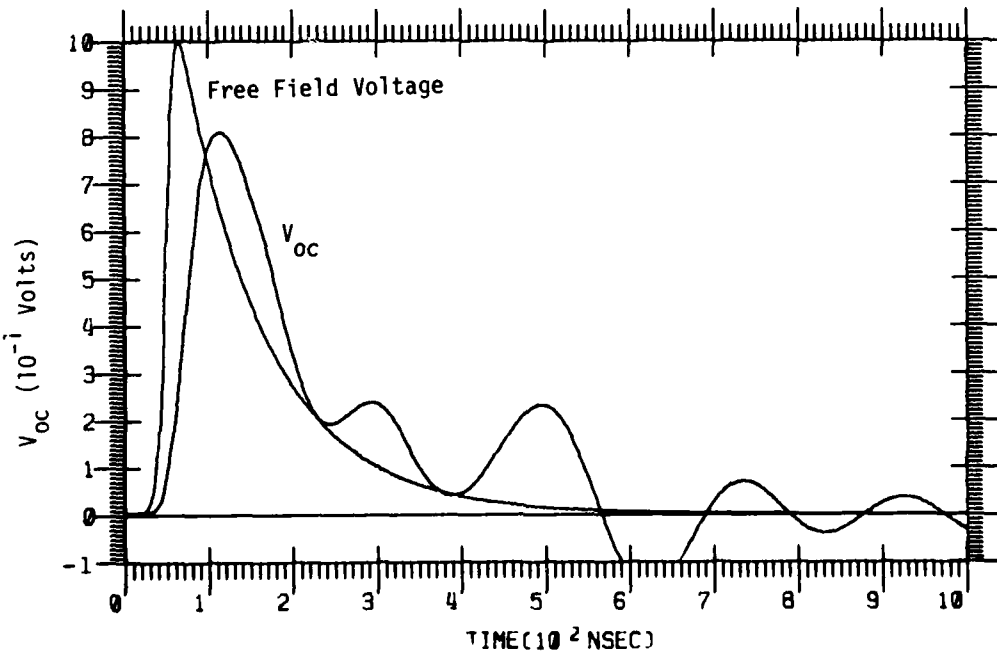


Figure 16b. Open Circuit Voltage for Horizontal Case 2
Electric Field (1 μ sec)

be to distort any measurement of the vertical component of a free space field. The significance of this distortion can be seen by the following calculations for a free field polarized at 30° relative to the vertical.

3.3 30° POLARIZED FIELD

For a free field polarized at 30° to the vertical (see Figure 12) the antenna open circuit voltage is a combination of both the vertical component coupling directly with the antenna and the horizontal component cross coupling with the antenna by means of charge distributions induced on the aircraft body. In calculating the antenna open circuit voltage that results from such a polarized field, it is important to note the relative orientation of the vertical and horizontal components. In our calculation we have the field oriented 30° from the vertical in the forward (referenced to the aircraft) direction. For this orientation, the antenna voltages for both the vertical and horizontal components add, and the results are shown in Figures 17a and 17b for case 1 and in Figure 18a and 18b for case 2. However, had we oriented the field 30° from the vertical in the aft direction, then the antenna voltage from the horizontal component of the field would be opposite in sign from that seen by the vertical component and some cancellation would have resulted.

For comparison, the voltage that the vertical component alone would have generated with an antenna effective height equal to the physical height has also been plotted on the graphs. In observing Figures 17 and 18, we see that the antenna open circuit voltage is considerably different in shape from the free field voltage. This distortion has been mainly caused by the cross coupling of the horizontal component of the field with the antenna.

The point to be made from these calculations is that because of the frequency dependence of the effective height and because of the cross coupling of the horizontal component of the incident field, the recorded voltage from a monopole antenna on an aircraft does not adequately measure the vertical component of an incident electric field.

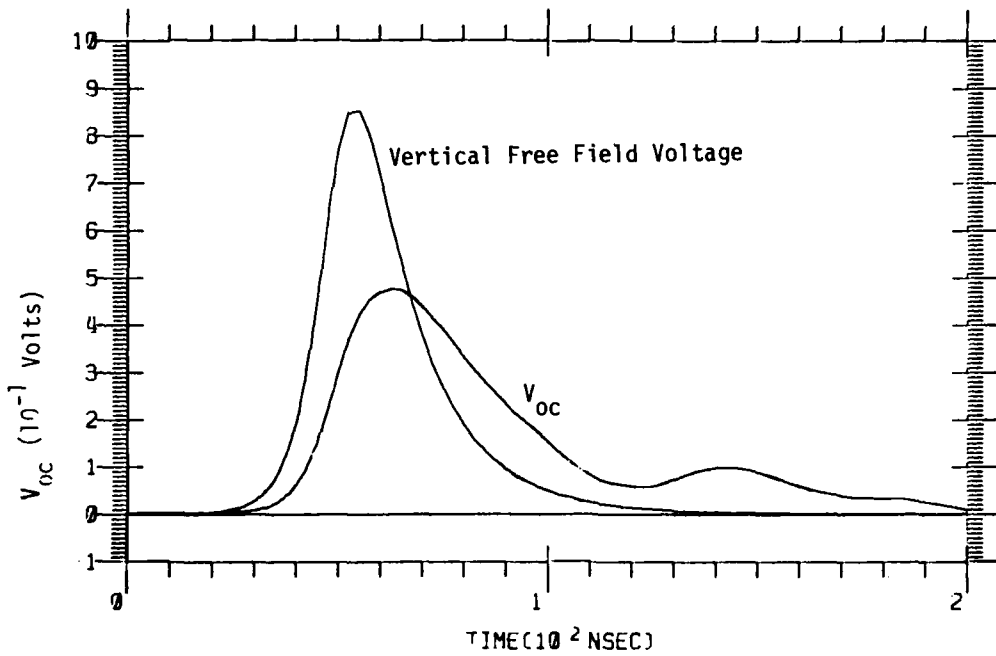


Figure 17a. Open Circuit Voltage for 30° Polarized Case 1
Electric Field (200 nsec)

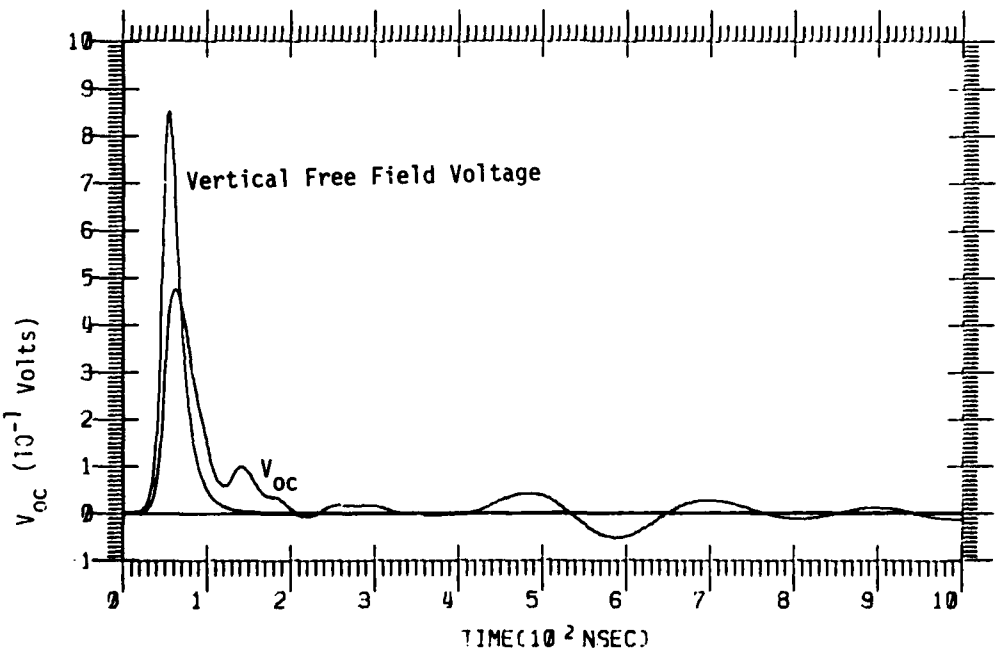


Figure 17b. Open Circuit Voltage for 30° Polarized Case 1
Electric Field (1 μ sec)

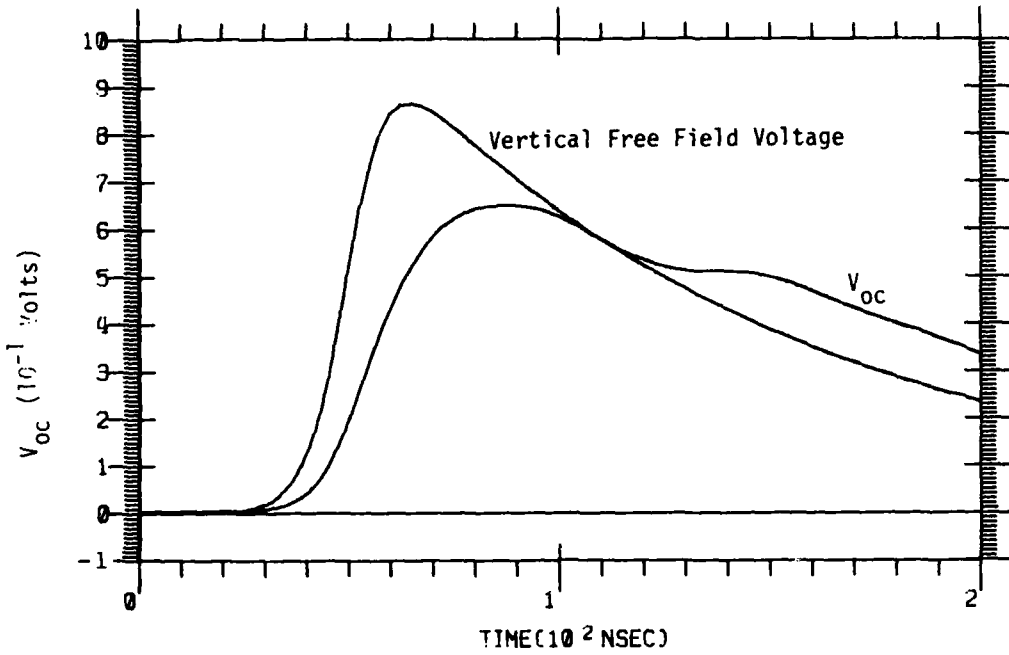


Figure 18a. Open Circuit Voltage for 30° Polarized Case 2
Electric Field (200 nsec)

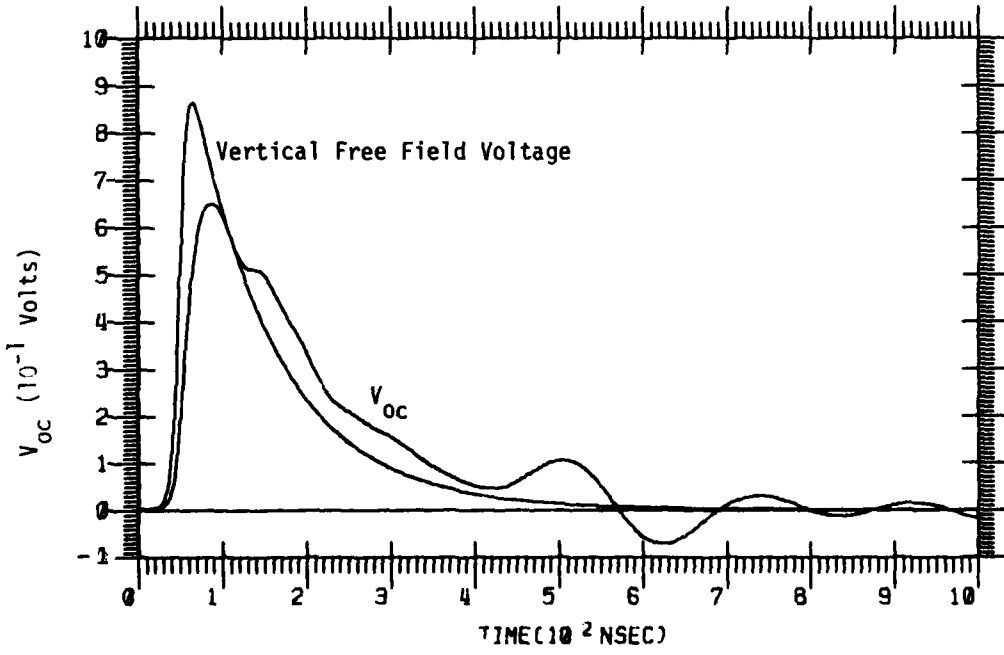


Figure 18b. Open Circuit Voltage for 30° Polarized Case 2
Electric Field (1 μ sec)

SECTION IV.

CONCLUSIONS

Our ability to make accurate electric field measurements from aircraft platforms has been questioned because of two contaminating effects, which are referred to as the aircraft response. First, the enhancement of the normal electric field by the conducting surface of the aircraft is affected by the finite dimensions of the aircraft and is not readily known. Second, there is a low frequency cross-coupling of horizontal electric field components with a vertical antenna due to the aircraft structure.

The Boeing measurement program has provided amplitude data on the effective heights for a single antenna location on a single aircraft type. This data is useful in scoping the magnitude of the above two problems. For the vertical electric field response measured, the effect of the reflected field from the conducting aircraft surface was not to enhance the low frequency effective height, but rather to create aircraft structure resonances in the antenna voltage. This lack of enhancement in the low frequency effective height, while at first glance surprising, is not unreasonable when one considers that the antenna is located near the front of the fuselage and thus the net reflected field can be appreciably diminished. For the horizontal electric field response measured, the effect of the aircraft structure was to provide a low frequency (less than 10 MHz) coupling which was larger than the vertical coupling by up to a factor of two.

To understand the measurement capability of a particular electric field antenna on an aircraft, it is necessary to have the complex frequency effective height for the polarizations of interest. In this regard, the Boeing measurements of the phase were not adequate because of the ambiguities associated with the data reduction. However, given the amplitude data as a function of frequency, we have shown that it is possible to calculate a phase through the use of a causality constraint on the data. The use of such a calculated complex effective height for the C-130 aircraft antenna studied has indicated that the antenna open circuit voltage can be strongly influenced by the horizontal component of the incident field both in terms of its shape as well as its amplitude.

The net effect of the contamination by the horizontal component of the incident field is to question the use of blade antennas on aircraft for electric field measurements where better than a factor of two or three accuracy is desired. This is particularly important if frequency domain information over a broad spectrum is wanted.

APPENDIX A.

RELATIONSHIP BETWEEN PHASE AND AMPLITUDE UNDER CAUSALITY CONSTRAINT

There is a relationship between the phase and amplitude of a function in the Fourier domain if we require that the function vanish in the time domain for times less than zero. The constraint that the function vanish for negative times is just causality: i.e., no signal can be detected until it has arrived at the detector. The relationship resulting from this causality constraint is unique for a zero time delay or within a linear phase shift (i.e., ωt) for a given time delay and is known in electric circuit theory as the Bode minimum phase [A-1].

A.1 THEORY

The causality constraint can be expressed mathematically for a function $f(t)$ as:

$$f(t) = 0 \quad t < 0$$

$$f(t) = \int_{-\infty}^{\infty} \frac{d\omega}{2\pi} e^{-i\omega t} \tilde{f}(\omega) \quad t > 0 \quad (17)$$

where the value for $t > 0$ is just the inverse Fourier transform. Since the Fourier transform is defined for both positive and negative times, the properties of $\tilde{f}(\omega)$ that allow Eq. 17 to be satisfied are:

1. $\tilde{f}(\omega)$ is analytic in the upper half plane (u.h.p.) of the complex ω plane.
2. $\tilde{f}(\omega) \rightarrow 0$ uniformly as $|\omega| \rightarrow \infty$.

The necessity of these two conditions can be shown by the following:

For $t < 0$

$$f(t) = \int_{-\infty}^{\infty} \frac{d\omega}{2\pi} e^{-i\omega t} \tilde{f}(\omega). \quad (18)$$

If $\tilde{f}(\omega)$ goes to zero uniformly as $|\omega|$ becomes large, then by using Jordan's Lemma [A-2], we can close the contour in the u.h.p. at $|\omega| \rightarrow \infty$ and

$$f(t) = \oint_C \frac{dw}{2\pi} e^{-i\omega t} \tilde{f}(\omega) \quad (19)$$

where c is the contour shown in Figure 19.

Now, if $f(\omega)$ is analytic in the u.h.p. [i.e., if all poles and singularities are in the lower half plane (l.h.p.)], then by Cauchy's Theorem A-2], any closed contour integral of an analytic function is zero. Therefore,

$$\begin{aligned} f(t) &= 0 \\ \text{for } t < 0. \end{aligned}$$

A.1.1 Relationship Between Real and Imaginary Parts of an Analytic Function

Using these properties of a complex function, $\tilde{f}(\omega)$, we can now derive certain relations between the real and imaginary parts. Let

$$\tilde{f}(\omega) = u(\omega) + i v(\omega); \quad (20)$$

then, since $\tilde{f}(\omega)$ is analytic within the contour c of Figure 19, we have from Cauchy's Integral Formula [A-3]:

$$\tilde{f}(\omega) = \frac{1}{2\pi i} \oint_C \frac{dz \tilde{f}(z)}{(z-\omega)}. \quad (21)$$

Next, because of the second property of $\tilde{f}(\omega)$, i.e., that it converges uniformly to zero for large ω , we can reduce Eq. 21, to a principal value line integral over the real axis; or

$$\tilde{f}(\omega) = \frac{P}{\pi i} \int_{-\infty}^{\infty} dz \frac{\tilde{f}(z)}{(z-\omega)}. \quad (22)$$

If we now equate the real and imaginary sides of Eq. 22, we have

$$u(\omega) = \frac{P}{\pi} \int_{-\infty}^{\infty} dz \frac{v(z)}{(z-\omega)} \quad (23a)$$

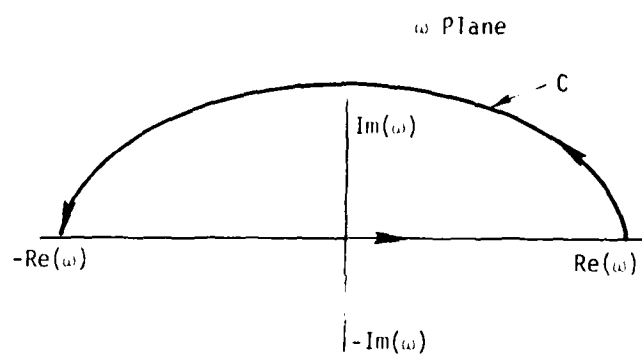


Figure 19. Contour of Integration in Complex ω Plane

$$v(\omega) = \frac{-P}{\pi} \int_{-\infty}^{\infty} dz \frac{u(z)}{(z-\omega)} . \quad (23b)$$

We can further reduce these relations to integrals over half the real axis and eliminate the principal value integral by removing the singularity at $z = \omega$. Noting that

$$P \int_{-\infty}^{\infty} \frac{dz}{z-\omega} = 0.$$

so that

$$P \int_{-\infty}^{\infty} \frac{dz}{z-\omega} \tilde{f}(\omega) = 0$$

and that

$$u(\omega) = \int_{-\infty}^{\infty} dt \cos(\omega t) f(t) = u(-\omega)$$

$$v(\omega) = \int_{-\infty}^{\infty} dt \sin(\omega t) f(t) = -v(-\omega)$$

we have

$$u(\omega) = \frac{2}{\pi} \int_0^{\infty} dz \frac{[z \cdot v(z) - \omega \cdot v(\omega)]}{(z^2 - \omega^2)} \quad (24)$$

and

$$v(\omega) = -\frac{2\omega}{\pi} \int_0^{\infty} dz \frac{[u(z) - u(\omega)]}{(z^2 - \omega^2)} . \quad (25)$$

Another useful form for showing the relationship between the real and imaginary parts can be obtained by integrating Eqs. 24 and 25, by parts. Then we have

$$u(\omega) = \frac{1}{\pi\omega} \int_0^\infty dz \ln \frac{z+\omega}{z-\omega} [v(z) - z v'(z)] \quad (26)$$

$\alpha v \phi$

$$v(\omega) = \frac{-1}{\pi} \int_0^\infty dz \ln \frac{z+\omega}{z-\omega} \cdot u'(z) \quad (27)$$

As will be noted in Section A.2, by using Equations 24 and 25 or 26 and 27, certain fundamental properties of the real versus imaginary parts can be determined.

A.1.2 Relationship Between Amplitude and Phase for Causal Function

We showed in Section A.1.1 that if $\tilde{f}(\omega)$ was analytic in the u.h.p., then the function $f(t)$ was causal (i.e., $f(t) = 0$ for $t < 0$). In addition, we showed that there is a relationship between the real and imaginary parts of $\tilde{f}(\omega)$ when $\tilde{f}(\omega)$ is analytic. We can now make use of this information to derive a relation between the amplitude and phase of such a complex function. Let

$$\tilde{f}(\omega) = u(\omega) + i v(\omega) = A(\omega) e^{i\phi(\omega)} \quad (28)$$

where

$$A(\omega) = [u^2 + v^2]^{1/2}$$

$$\phi(\omega) = \tan^{-1}(v/u)$$

or

$$A(\omega) = [f^* f]^{1/2}$$

$$\phi(\omega) = \tan^{-1}[(f-f^*)/i(f+f^*)].$$

We may also define a new function $g(\omega)$ such that

$$\tilde{f}(\omega) = e^{g(\omega)}; \quad (29)$$

thus,

$$g(\omega) = \ln [A(\omega)] + i \phi(\omega). \quad (30)$$

We will now show that $g(\omega)$ has the properties of analyticity and uniform convergence; then we can use the relations between real and imaginary parts to provide the relations between amplitude and phase.

1. Analyticity

If $\tilde{f}(\omega)$ is analytic within a region of the complex ω plane, then $g(\omega)$, equal to $\ln[\tilde{f}(\omega)]$, is analytic except where $|\tilde{f}(\omega)| \rightarrow 0$.

We can prove this statement by considering the Cauchy-Riemann conditions [A-3] for an analytic function, i.e.,

if

$$\tilde{f}(\omega) = u(\omega) + i v(\omega)$$

and

$$\omega = x + iy,$$

then a necessary condition for analyticity of $\tilde{f}(\omega)$ is

$$\frac{\partial u}{\partial x} = \frac{\partial v}{\partial y} \quad \text{and} \quad \frac{\partial u}{\partial y} = -\frac{\partial v}{\partial x} \quad (31)$$

and a sufficient condition is that the derivatives are continuous.

Let $g(\omega) = R(\omega) + i I(\omega)$.

Then, $u(\omega) = e^{R(\omega)} \cos [I(\omega)]$

and $v(\omega) = e^{R(\omega)} \sin [I(\omega)]$.

Now, if $\tilde{f}(\omega)$ is analytic, then we have

$$\frac{\partial}{\partial x} \left[e^{R(\omega)} \cos I(\omega) \right] = -\frac{\partial}{\partial y} \left[e^{R(\omega)} \sin I(\omega) \right] \quad (32)$$

and

$$\frac{\partial}{\partial y} \left[e^{R(\omega)} \cos I(\omega) \right] = -\frac{\partial}{\partial x} \left[e^{R(\omega)} \sin I(\omega) \right]. \quad (32)$$

Therefore, after manipulating these two equations we have

$$\begin{aligned} e^{R(\omega)} \frac{\partial R(\omega)}{\partial x} - \frac{\partial I(\omega)}{\partial y} &= 0 \\ e^{R(\omega)} \frac{\partial R(\omega)}{\partial y} + \frac{\partial I(\omega)}{\partial x} &= 0. \end{aligned} \quad (33)$$

As long as $R(\omega) > -\infty$, the Cauchy-Riemann conditions are met and the derivatives of R and I are continuous since $A(\omega)$ and $\phi(\omega)$ have no discontinuities. Thus, $g(\omega)$ is analytic within the region that $f(\omega)$ is analytic. However, as $|\omega| \rightarrow \infty$, $f(\omega) \rightarrow 0$ and $\ln[f(\omega)] \rightarrow -\infty$, so $g(\omega)$ has a singularity at $|\omega| = \infty$.

We can transform this singularity at ∞ to one at the origin if we know how $f(\omega) \rightarrow 0$ as $\omega \rightarrow \infty$.

If $\tilde{f}(\omega) \rightarrow 0$ as $\tilde{f}_\infty(\omega) = A_\infty(\omega) e^{i\phi_\infty}$,

$$|\omega| \rightarrow \infty$$

then we can create a new function $h(\omega)$ where

$$h(\omega) = g(\omega) - \ln[\tilde{f}_\infty(\omega)] = \ln[A(\omega)/A_\infty(\omega)] + i(\phi - \phi_\infty). \quad (34)$$

Now, if $\tilde{f}_\infty(\omega)$ is analytic in the u.h.p. except for simple poles on the real axis (which we can handle by principal value integrals), then $h(\omega)$ has the properties that it is analytic in the u.h.p. with only logarithmic singularities on the real axis and converges to zero uniformly as $|\omega| \rightarrow \infty$. This new function can be used to relate the amplitude and phase with Equations 24 and 25 as:

$$\ln \left[A(\omega) / A_\infty(\omega) \right] = \frac{2}{\pi} \int_0^\infty dz \frac{z [\phi(z) - \phi_\infty(z)] - \omega [\phi(\omega) - \phi_\infty(\omega)]}{(z^2 - \omega^2)} \quad (35)$$

and

$$[\phi(\omega) - \phi_\infty(\omega)] = \frac{2\omega}{\pi} \int_0^\infty dz \frac{\ln[A(z)/A_\infty(z)] - \ln[A(\omega)/A_\infty(\omega)]}{(z^2 - \omega^2)} \quad (36)$$

A.2 APPLICATION OF CAUSAL PHASE AND AMPLITUDE RELATIONSHIP

The principal uses of Eq. 34 and 35 in this report are to check and correct the phase and amplitude data over a frequency regime $\omega_0 < \omega < \omega_1$ and to provide a basis for extrapolating that data without generating any causal errors in the transform. In this regard, it is important to note a few trends in the relations between phase and amplitude.

A.2.1 Constant Amplitude

When $A(\omega)$ is constant for $0 < \omega < \omega_0$, then from Eq. 35, we see that the phase will increase linearly from zero. This can be shown as follows:

$$A(\omega) = A_0 \quad \omega < \omega_0.$$

Then Equation 36 becomes

$$\begin{aligned} \phi(\omega) - \phi_\infty &= \frac{-2\omega}{\pi} \left\{ \int_0^{\omega_0} dz \frac{\ln[A_\infty(\omega)/A_\infty(z)]}{(z^2 - \omega^2)} \right. \\ &\quad \left. \omega < \omega_0 \right. \\ &+ \int_{\omega_0}^\infty dz \frac{\ln([A(z) \cdot A_\infty(\omega)]/[A_0 \cdot A_\infty(z)])}{(z^2 - \omega^2)} \end{aligned} \quad (37)$$

or

$$\phi(\omega) = \left\{ \phi_\infty - \frac{2\omega}{\pi} \int_0^\infty dz \frac{\ln[A_\infty(\omega)/A_\infty(z)]}{(z^2 - \omega^2)} \right\} - \frac{2\omega}{\pi} \int_0^\infty dz \frac{\ln[A(z)/A_0]}{(z^2 - \omega^2)} \quad (38)$$

$\omega < \omega_0$

but

$$\phi_\infty = \frac{2\omega}{\pi} \int_0^\infty \frac{dz}{(z^2 - \omega^2)} \ln[A_\infty(\omega)/A_\infty(z)]. \quad (39)$$

Therefore,

$$\phi(\omega) = \frac{-2\omega}{\pi} \int_{\omega_0}^{\infty} dz \frac{\ln[A(z)/A_0]}{(z^2 - \omega^2)} \quad (40)$$

or since $\omega < \omega_0 \leq z$

$$\phi(\omega) \approx \omega \cdot \left\{ \frac{-2}{\pi} \int_{\omega_0}^{\infty} \frac{dz}{z^2} \ln[A(z)/A_0] \right\} \quad (41)$$

Thus, if we have a constant amplitude, the phase will rise linearly with ω as shown in Figure 20.

A.2.2 Amplitude Falloff

If $A(\omega)$ goes to zero like $1/\omega^m$, then the phase shift at $\omega = \infty$ can be determined to be $m \frac{\pi}{2}$. To show this, we look at the relation

$$\phi_{\infty} = \frac{-2\omega}{\pi} \int_0^{\infty} dz \frac{\ln[\omega^m/z^m]}{(z^2 - \omega^2)}, \quad (42)$$

or

$$\phi_{\infty} = \left(\frac{2\omega}{\pi} \right)^m \int_0^{\infty} \frac{dz}{\omega^2} \frac{\ln[z/\omega]}{(z^2/\omega^2 - 1)}. \quad (43)$$

Let $u = z/\omega$.

Then

$$\phi_{\infty} = \frac{2m}{\pi} \left\{ \int_0^1 du \frac{\ln(u)}{(u^2 - 1)} + \int_1^{\infty} du \frac{\ln(u)}{(u^2 - 1)} \right\} \quad (44)$$

or

$$\phi_{\infty} = \frac{4m}{\pi} \int_0^1 du \frac{\ln(u)}{(u^2 - 1)}. \quad (45)$$

Therefore,

$$\phi_{\infty} = \frac{4m}{\pi} \left(\frac{\pi^2}{8} \right) \quad (46)$$

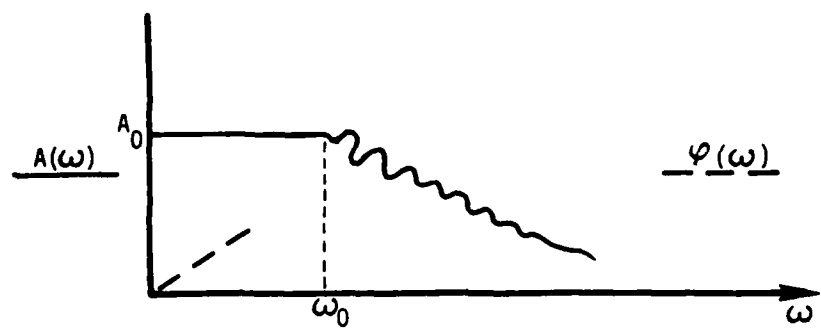


Figure 20. Phase for a Constant Amplitude

or

$$\phi_{\infty} = m \frac{\pi}{2} \quad (47)$$

To understand how the phase approaches this value, ϕ_{∞} , we can look at the value of $\phi(\omega)$ when ω becomes large. When $A(\omega) \approx A_{\infty}(\omega)$ for $\omega > \omega_1$, Equation 35 becomes

$$\phi(\omega) - \phi_{\infty}(\omega) \approx - \frac{2\omega}{\pi} \int_0^{\omega_1} dz \frac{\ln[A(z)/A_{\infty}(z)]}{(z^2 - \omega^2)} \quad (48)$$

or

$$\phi(\omega) \approx \phi_{\infty} + \frac{1}{\omega} \cdot \left\{ \frac{2}{\pi} \int_0^{\omega_1} dz \ln[A(z)/A_{\infty}(z)] \right\}. \quad (49)$$

Thus, $\phi(\omega) \rightarrow \phi_{\infty}$ like $1/\omega$ and approaches from above or below depending on whether $A(z)$ is greater than or less than $A_{\infty}(z)$ over the range of integration. Figure 21 shows this trend.

A.2.3 Phase in Region of Amplitude Variation

To help understand the variation in phase for rapid amplitude variations, we can look at Equation 24 and 25 for different conditions.

First, let us consider the case where the phase varies from $\pm\pi$ to 0 as shown in Figure 21a.

Case 1: $\phi(\omega) = \pi \cdot U(\omega_0 - \omega)$

$$\phi'(\omega) = -\pi \delta(\omega_0 - \omega)$$

Using Equation 24, where $v(\omega) = [\phi(\omega) - \phi_{\infty}(\omega)]$ and $u(\omega) = \ln [A(\omega)/A_{\infty}(\omega)]$, we have

$$\ln[A(\omega)/A_{\infty}(\omega)] = \frac{1}{\pi\omega} \int_0^{\infty} dz \ln \left| \frac{z+\omega}{z-\omega} \right| [\pi U(\omega_0 - z) - z \pi \delta(\omega_0 - z)]. \quad (50)$$

Therefore,

$$\begin{aligned} \ln[A(\omega)/A_{\infty}(\omega)] &= \frac{1}{\omega} \left\{ \int_0^{\omega_0} dz \ln \left| \frac{z+\omega}{z-\omega} \right| - \omega_0 \ln \left| \frac{\omega_0 - \omega}{\omega_0 + \omega} \right| \right\} \\ &= \frac{1}{\omega} \left\{ \omega \ln \left| \omega_0^2 - \omega^2 \right| - \omega \ln \omega^2 \right\} \end{aligned} \quad (51)$$

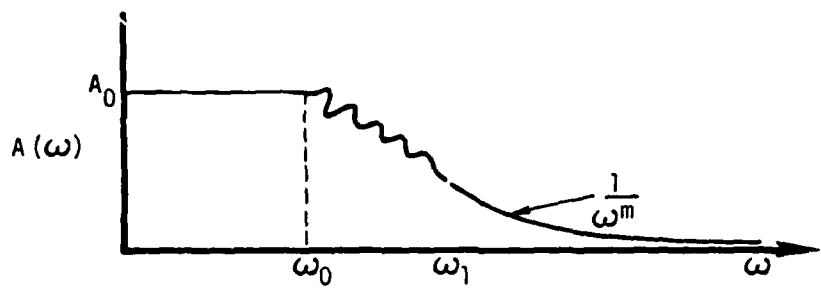


Figure 21a. Amplitude Function

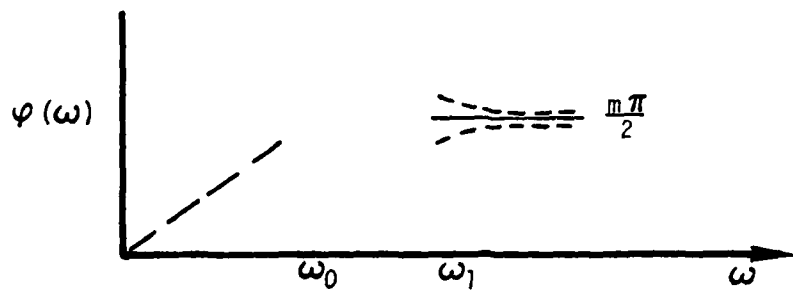


Figure 21b. Phase Function

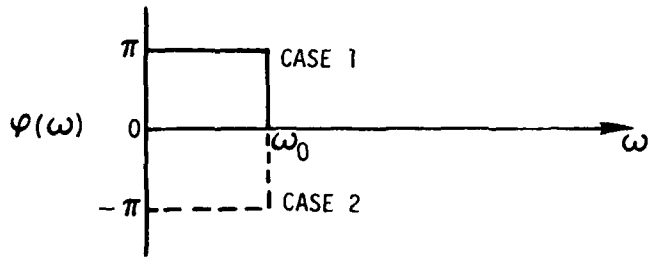


Figure 22a. π Shift in Phase

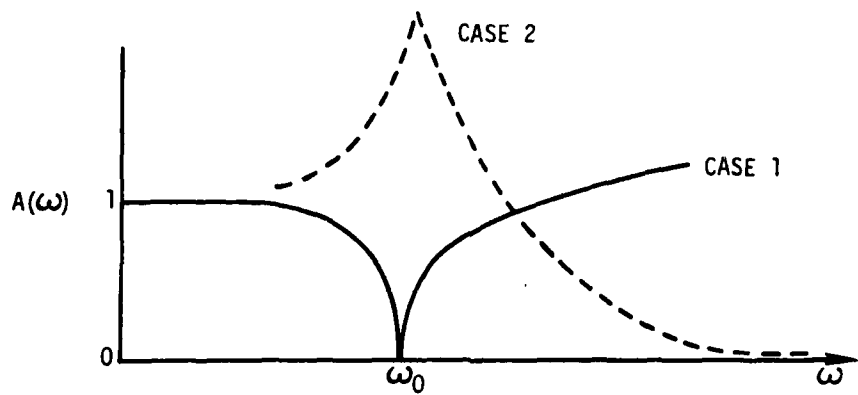


Figure 22b. Amplitude for π Shift in Phase

or

$$\ln A(\omega)/A_\infty(\omega) = \ln \left| \frac{\omega_0^2 - \omega^2}{\omega^2} \right|. \quad (52)$$

Thus,

$$A(\omega) = \left| \frac{\omega_0^2 - \omega^2}{\omega^2} \right| \quad (53)$$
$$A_\infty(\omega) = \frac{\omega^2}{\omega_0^2}.$$

Figure 22b shows this form. Thus for a phase shift from $+\pi$ to 0, the amplitude goes through a null.

Case 2: $\phi(\omega) = -\pi u(\omega_0 - \omega)$

$$\phi'(\omega) = \pi \delta(\omega_0 - \omega)$$

For this case we note that Equation 24 becomes

$$\begin{aligned} \ln [A(\omega)/A_\infty(\omega)] &= \frac{1}{\pi} \left\{ - \int dz \ln \left| \frac{z+\omega}{z-\omega} \right| + \omega_0 \ln \left| \frac{\omega_0+\omega}{\omega_0-\omega} \right| \right\} \\ &= \ln \left| \frac{\omega^2}{\omega_0^2 - \omega^2} \right| \end{aligned} \quad (54)$$

Therefore,

$$A(\omega) = \frac{\omega_0^2}{|\omega_0^2 - \omega^2|} \quad (55)$$
$$A_\infty(\omega) = \frac{\omega_0^2}{\omega^2}$$

Thus for a π shift in phase with a positive slope, the amplitude goes through a resonance as shown in Figure 22b.

REFERENCES

- A-1. H. W. Bode, Network Analysis and Feedback Amplifier Design, D. Van Nostrand Company, Inc., Princeton, New Jersey, 1945.
- A-2. E. T. Wittaker and G. N. Watson, A Course of Modern Analysis, Cambridge University Press, London, England, 1963.
- A-3. P. M. Morse and H. Feshback, Methods of Theoretical Physics, McGraw-Hill Book Company, Inc., New York, New York.

APPENDIX B

DIFFICULTIES IN USING THE MEASURED EFFECTIVE HEIGHT DATA

Difficulties were encountered in using the Boeing effective height data to study the effect of the aircraft response on the measuring of vertical electric fields. The major difficulty was in the lack of a causal relationship between the phase and the amplitude functions. This lack of causality is believed to be due to the ambiguity in the phase data reduction and in misinterpretation of the original lack of agreement between the 45° data and the vertical and horizontal data.

B.1 CORRELATION OF 45° DATA WITH THE VERTICAL AND HORIZONTAL DATA

The Boeing measurement program on the effective height of a 1-m blade antenna on a C-130 aircraft produced amplitude and phase data for three polarizations: vertical, horizontal and at 45° (Ref. B-1). Figure 23 shows the orientation of these polarizations relative to the aircraft and the antenna. The estimates of the errors in these measurements were ± 2 dB for the amplitude and $\pm 30^\circ$ for the phase. As part of a review for DNA on the preliminary draft (Ref. B-3) of the measurement results, we noted that the horizontal and vertical data did not correlate with the 45° data. Based on our comments, Boeing reviewed their data and concluded that because of the $\pm 180^\circ$ ambiguity in the phase measurements, a $\pm 90^\circ$ ambiguity resulted in their data reduction scheme between different scaled bands of the frequency region measured (Ref. B-2). Thus they changed the phase within certain scaled frequency bands of the data to bring the three polarizations into correlation. Figure 24 shows the scaled frequency bands used in the 0.5 to 100 MHz regions. We now believe that this change in the phase has resulted in a non-causal relationship between phase and amplitude.

In terms of our original comments on the non-correlation of the 45° data, we believe the major problem was in defining a consistent definition of positive and negative measurements. Referring to Figure 23, we note that if a field polarized like E_V is assumed to produce a positive signal from the antenna (V_V), then a field polarized like E_H will produce a negative signal (V_H). This can be easily seen in the limit of a low frequency quasi-static field. For a horizontal field pointed toward the tail, the electrons on the fuselage surface will move toward the front or cockpit creating a negative radial electric field near the antenna. Therefore, a field polarized like E_{45} in Figure 23

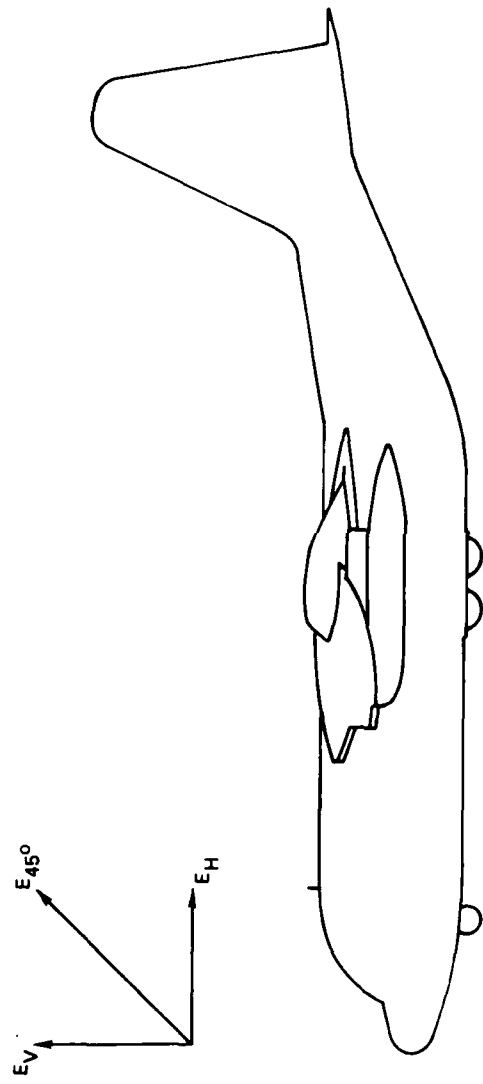


Figure 23. Orientation for Free Field Relative to the C-130 Model Aircraft

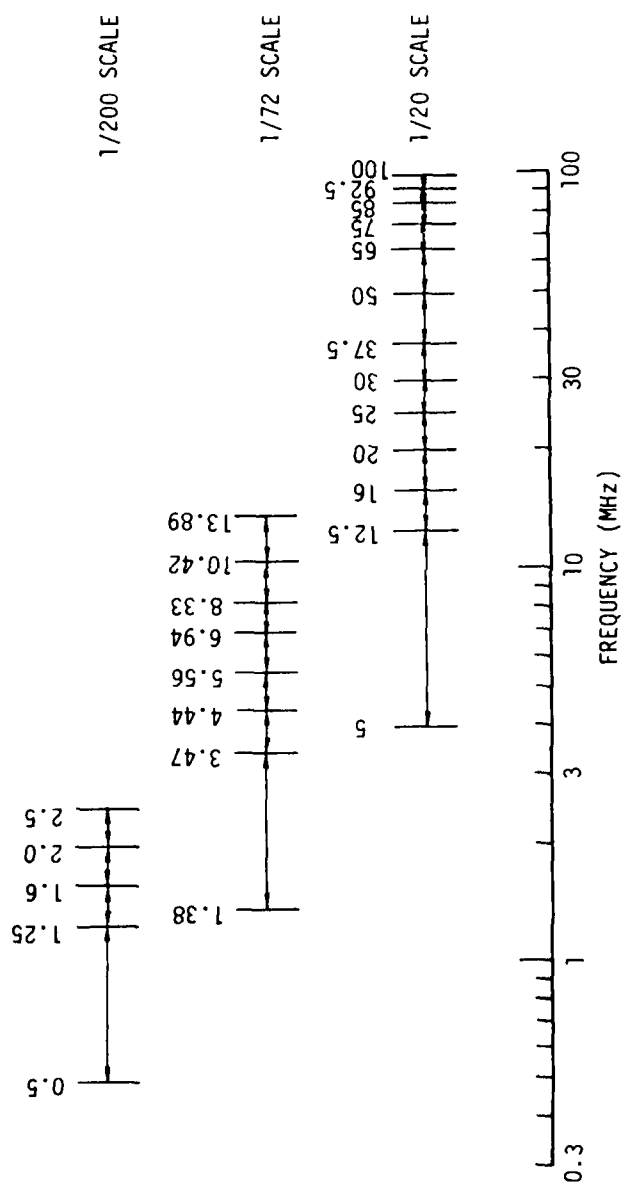


Figure 24. Scaled Frequency Bands

would produce canceling signals at the antenna and the V_{45} signal would be the difference between the V_H and V_V signals for low frequency or

$$V_{45} = |V_V| - |V_H|. \quad (56)$$

Figure 25 shows an overlay of the three sets of amplitude data measured by Boeing. On the graph we can see that $|V_H| \geq |V_V|$ for frequencies below 7 MHz and that at 4 MHz the amplitudes are equal which would account for the null seen in the V_{45} data. Thus the phase for the 45° data should have started at -180° , increased toward 0° near 7 MHz with a dip in the phase at 4 MHz to account for the nulling of the amplitude, as indicated by the relationship of phase and amplitude discussed in Appendix A. Figures 26 through 28 show the low frequency phase data presented by Boeing both in their preliminary draft (Ref. 3) and the final report (Ref. 1). As can be seen, the horizontal phase data was kept constant but both the vertical and 45° data changed. Note in Figure 27 that the vertical data below 4 MHz was shifted by 180° to account for the lack of correlation between the three polarizations. As was discussed above, this shift of 180° should have been attributed to the 45° data. In addition to this major change in the vertical data, there were also other changes made at higher frequencies. The point to be made is that the phase data as reported has considerable ambiguities which put in question its accuracy to $\pm 30^\circ$.

In the next two sections, we discuss our calculations which show that the effective height data is non-causal and the effect of that condition on the resulting open circuit voltage calculations. In Section B.4, using the measured amplitude data and the calculated phase functions discussed in the text, we present the calculated 45° amplitude and phase for comparison with the measured 45° data.

B.2 VERTICAL DATA CAUSALITY

As was noted above, the measurements of effective height phase and amplitude do not appear to be causal. To show this lack of causality, the frequency data was transformed to the time domain to observe the delta function response. The procedure for calculating this transform was as follows. First, the vertical data was extrapolated beyond the range of measurements to prevent the introduction of spurious signals in the time domain for sharp cut-offs in the frequency domain. For

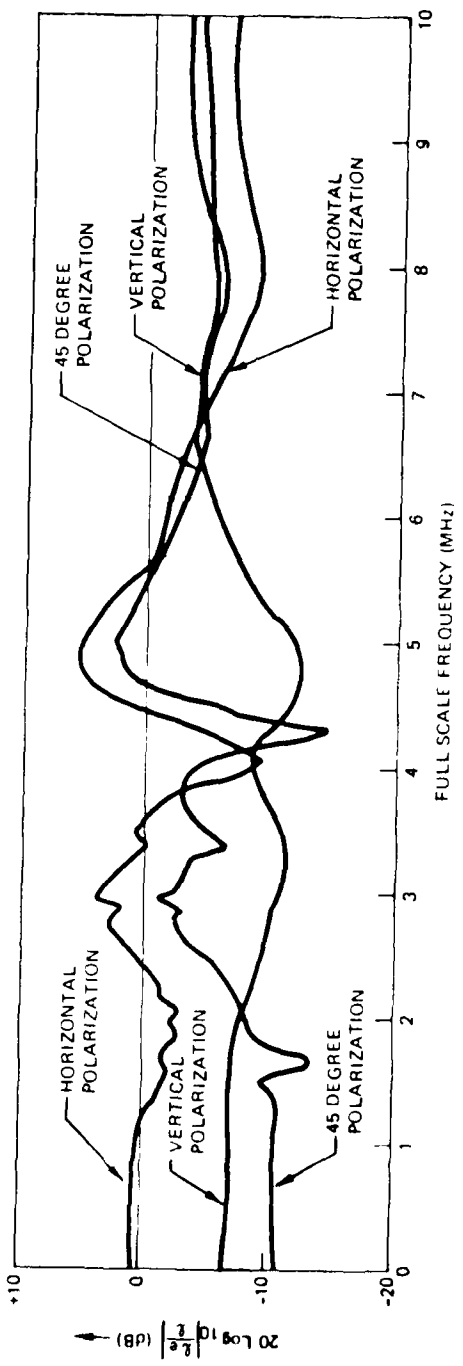


Figure 25. Effective Length Amplitude

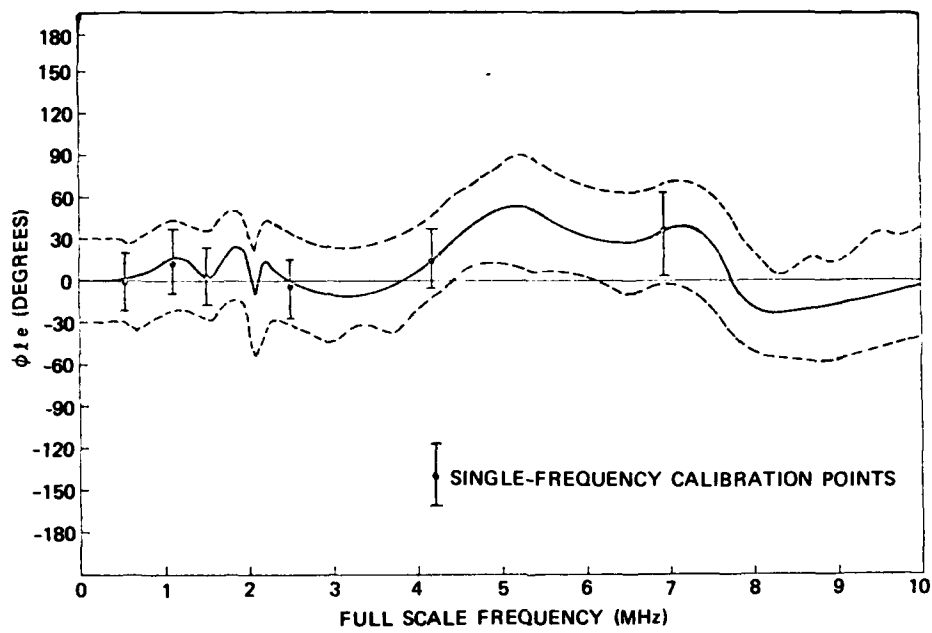


Figure 26a. Effective Length Phase Horizontal Polarization (Preliminary)

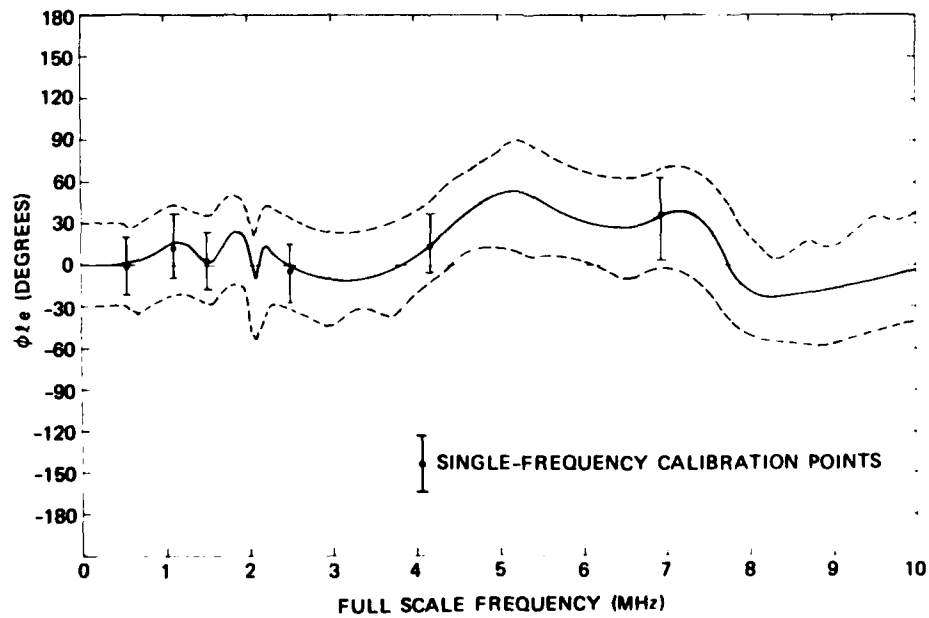


Figure 26 b. Effective Length Phase Horizontal Polarization (Final)

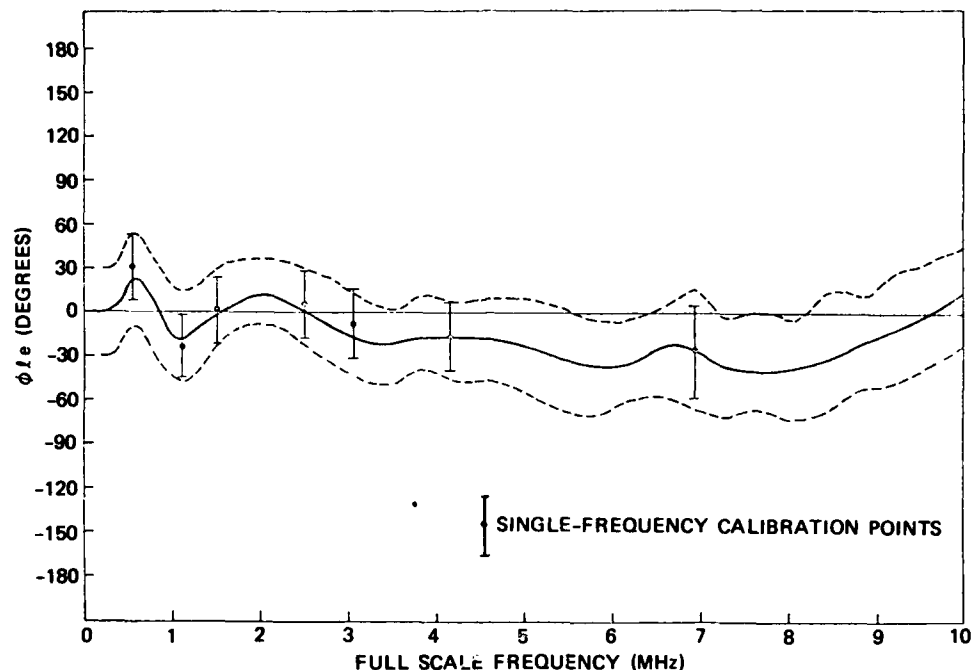


Figure 27a. Effective Length Phase Vertical Polarization (Preliminary)

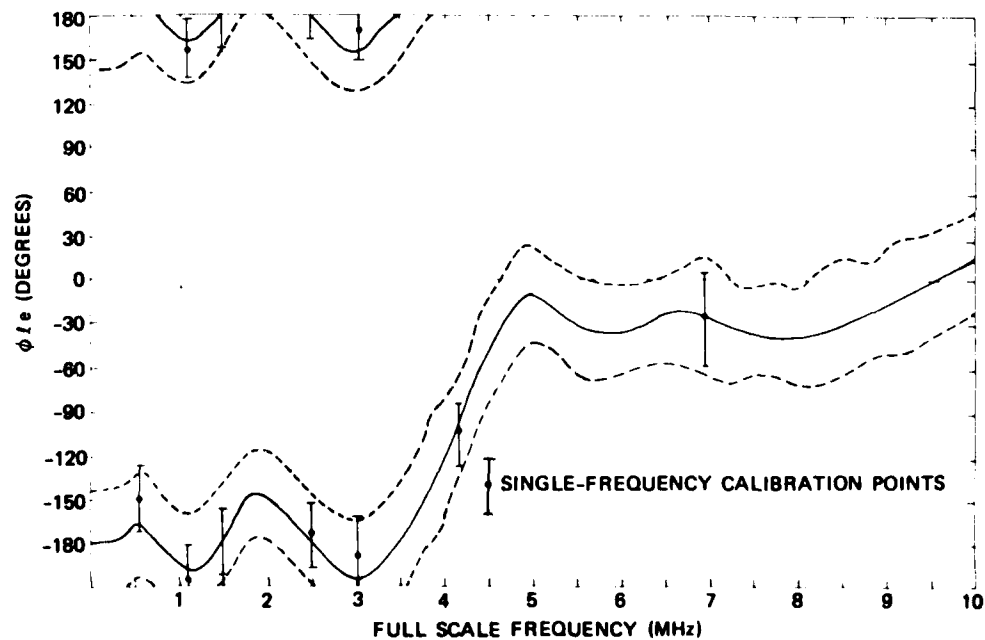


Figure 27 b. Effective Length Phase Vertical Polarization (Final)

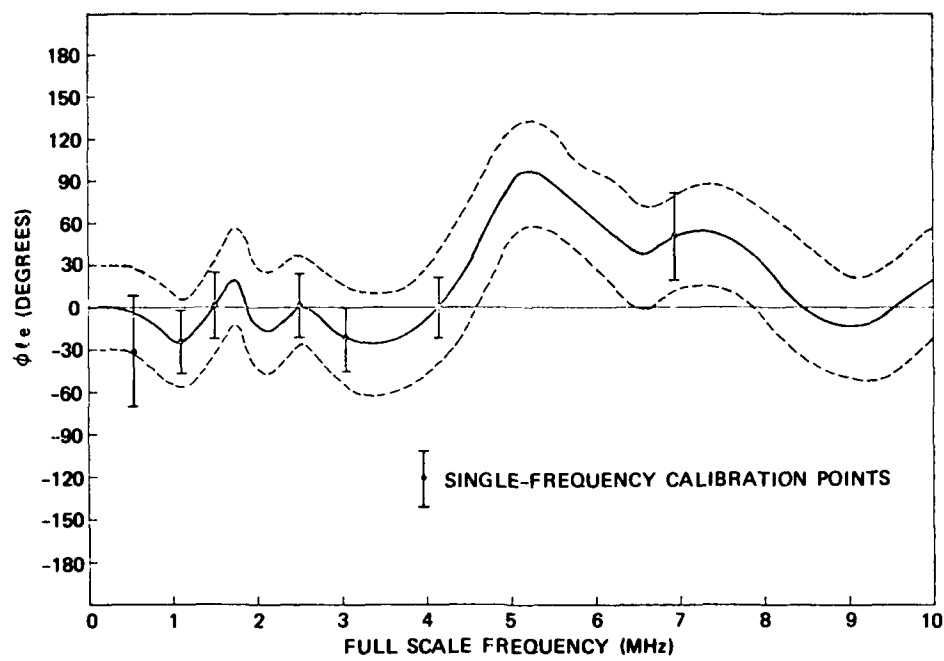


Figure 28a. Effective Length 45 Degree
Polarization (Preliminary)

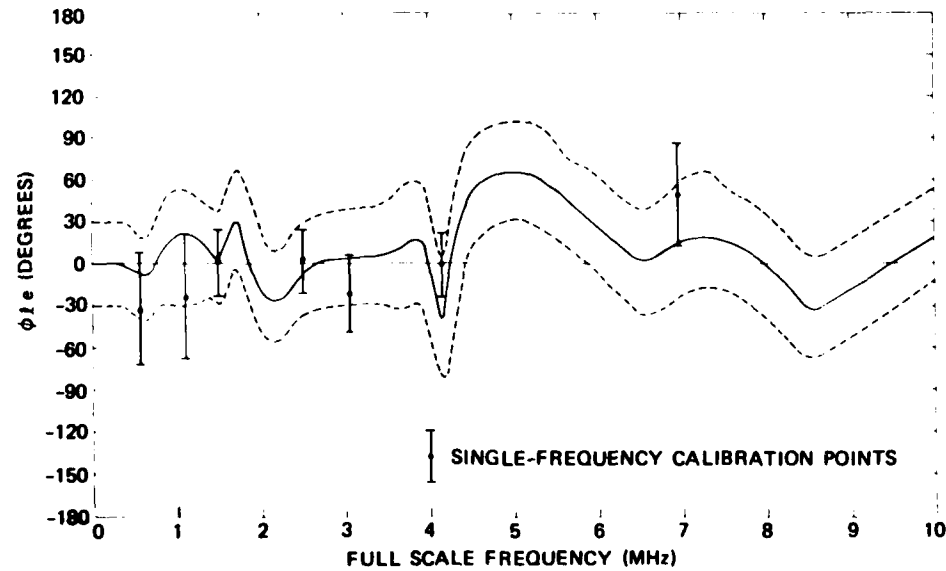


Figure 28b. Effective Length 45 Degree
Polarization (Final)

frequencies below 0.5 MHz the amplitude was assumed constant and the phase varied linearly to $-\pi$. For frequencies above 100 MHz, the amplitude was fit by the function discussed in Section II while the phase was extrapolated by the function

$$\phi(\omega < 2\pi \cdot 100 \text{ MHz}) = \tan^{-1} \left(\frac{\omega^2 - \omega_0^2}{\omega \Delta \omega} \right) \quad (57)$$

which corresponds to phase for an amplitude resonance of the form in Equation 10. The transform equation was

$$h_e(t) = \int_{\omega_N}^{\omega_N} \frac{d\omega}{2\pi} e^{-i\omega t} A(\omega) e^{i\phi(\omega)} \quad (58)$$

and was solved numerically by an FFT subroutine for ω_N equal to $2\pi \cdot 2\text{GHz}$. Figure 29 shows the resulting time history of h_e . The negative time values were obtained by changing the sign in the exponent of Eq. 58 from $-$ to $+$. Note the rather large precursor that results, which can significantly alter the calculation of an open circuit voltage. Also shown in Figure 29 is the delta function response for the amplitude data combined with the calculated phase function discussed in Section II. While there is still a precursor evident, its magnitude is less and its damps out quicker. As an example of the effect of this precursor on the open circuit voltage calculation, Figure 30 shows a voltage calculation of the Case 2 waveform discussed in Section III for both the reported vertical effective height and the amplitude combined with a calculated phase.

B.3 HORIZONTAL DATA

A calculation similar to the one discussed in Section B.2 was performed to look at the causality relationship of the horizontal data. Figure 31 shows the delta function response for the amplitude and phase reported versus a function utilizing the amplitude data with the causal phase function discussed in Section II. The calculation was performed using an FFT substantive to solve Equation 58, where the extrapolated values of the data were as follows. First, for frequencies below 0.5 MHz, the amplitude data was considered constant and the phase taken linearly to zero at $\omega = 0$. Second, for frequencies above 100 MHz, the amplitude was fit by the function given in Equation 12, which provided

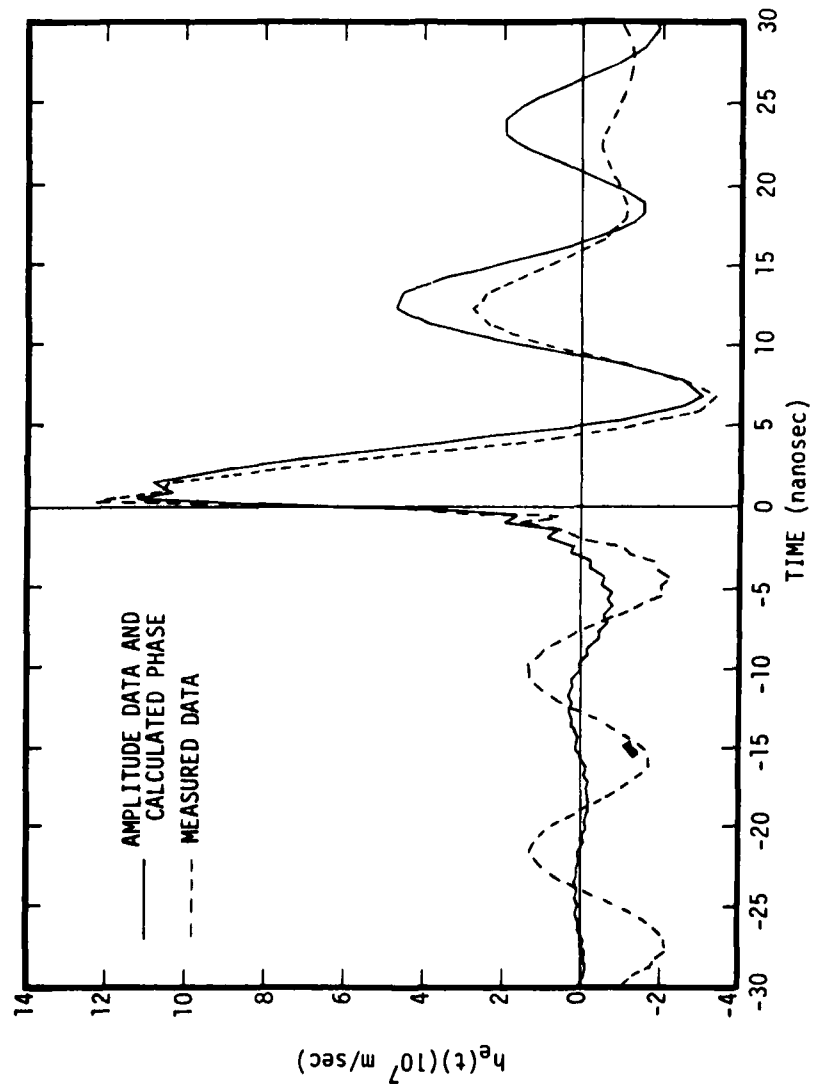


Figure 29. Vertical Polarization $h_e(t)$

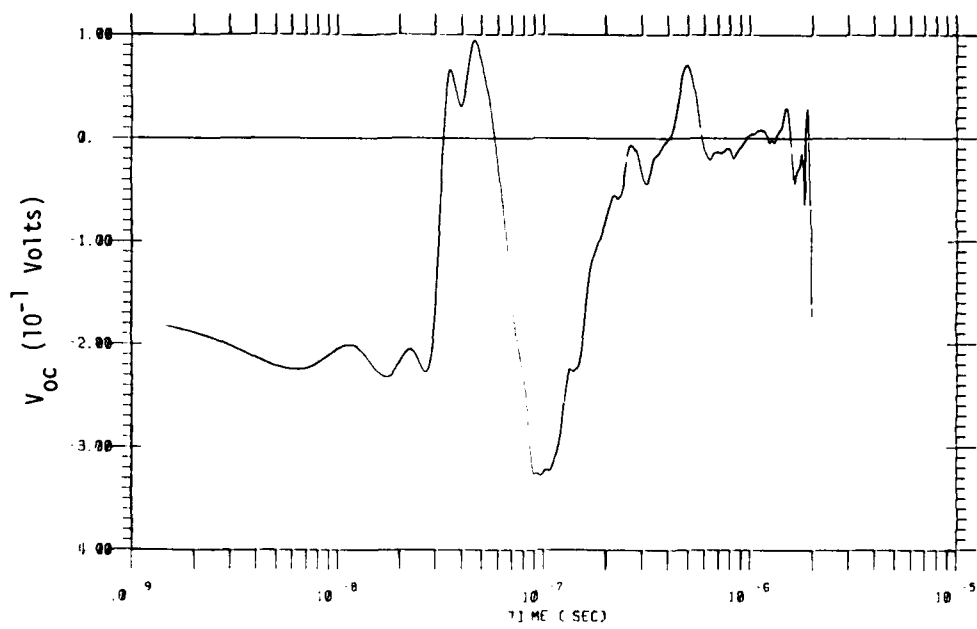


Figure 30a. V_{oc} for Measured Effective Height (Vertical Polarization)

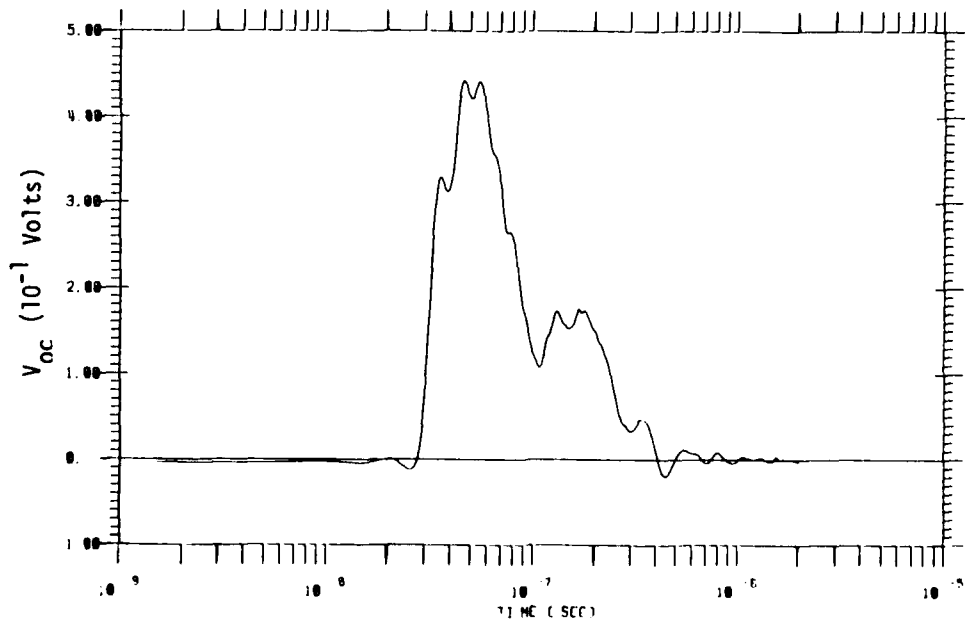


Figure 30b. V_{oc} for Measured Amplitude and Calculated Phase
(Vertical Polarization)

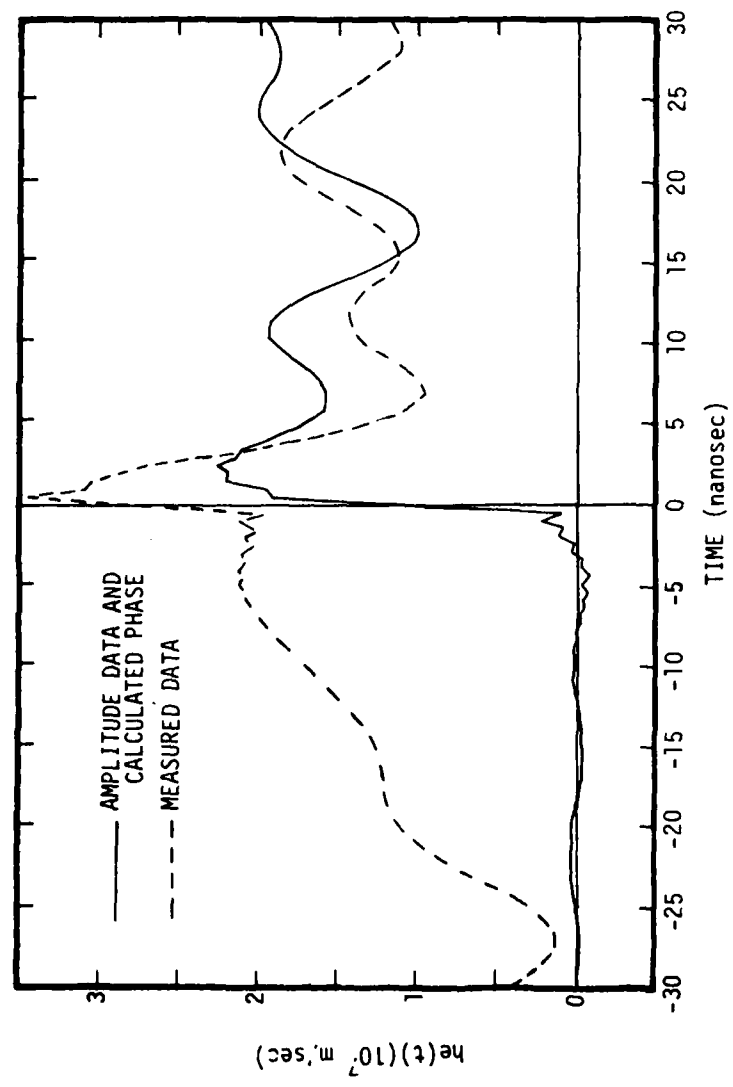


Figure 31. Horizontal Polarization $h_e(t)$

a smooth transition to a $1/\omega$ decay and the phase was extrapolated by

$$\phi(\omega < 2\pi \cdot 100 \text{ MHz}) = \tan^{-1} \omega/\omega_0 \quad (59)$$

where $\omega_0 = 2\pi \cdot 2 \text{ MHz}$.

The delta function response curve for the amplitude data and calculated phase function was calculated in the same manner.

Again, as an example of the effect of this precursor, calculations of the open circuit voltage were made using the measured phase and the calculated causal phase function. Figure 32 shows the results for an incident field of the form shown in Section III for Case 2.

Note in this case that although the precursor was larger, its effect was not as dramatic as for the vertical polarization, but its effect was still significant.

B.4 45° CALCULATION

As a further check on the accuracy of the antenna effective heights generated from the amplitude data and the causal relationship between phase and amplitude, we have combined the horizontal and vertical effective heights to compare with the measured 45° data. Using the orientation shown in Figure 23 and our definition of E_V producing a positive antenna output voltage, we have combined the effective heights in the following manner:

$$|h_{45}| = \left[|h_v|^2 + |h_h|^2 - 2|h_v h_h| \cos(\phi_v - \phi_h) \right]^{1/2} \cdot \cos(45) \quad (60)$$

and $\phi_{45} = \tan^{-1} \left\{ \frac{|h_v| \sin \phi_v - |h_h| \sin \phi_h}{|h_v| \cos \phi_v - |h_h| \cos \phi_h} \right\} \quad (61)$

Figure 33 shows the amplitude calculated from Equation 60. Figure 24 shows the phase from Equation 61. Also shown in Figure 33 is the error bound of the measured 45° amplitude data. At first glance, the comparison appears to be fairly good particularly in terms of the

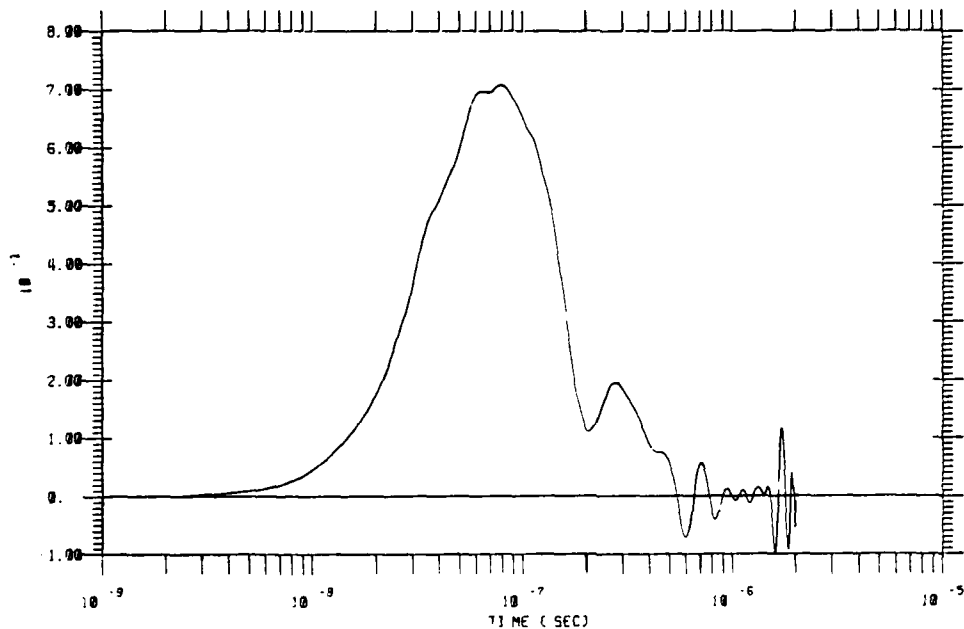


Figure 32a. V_{oc} for Measured Effective Height (Horizontal Polarization)

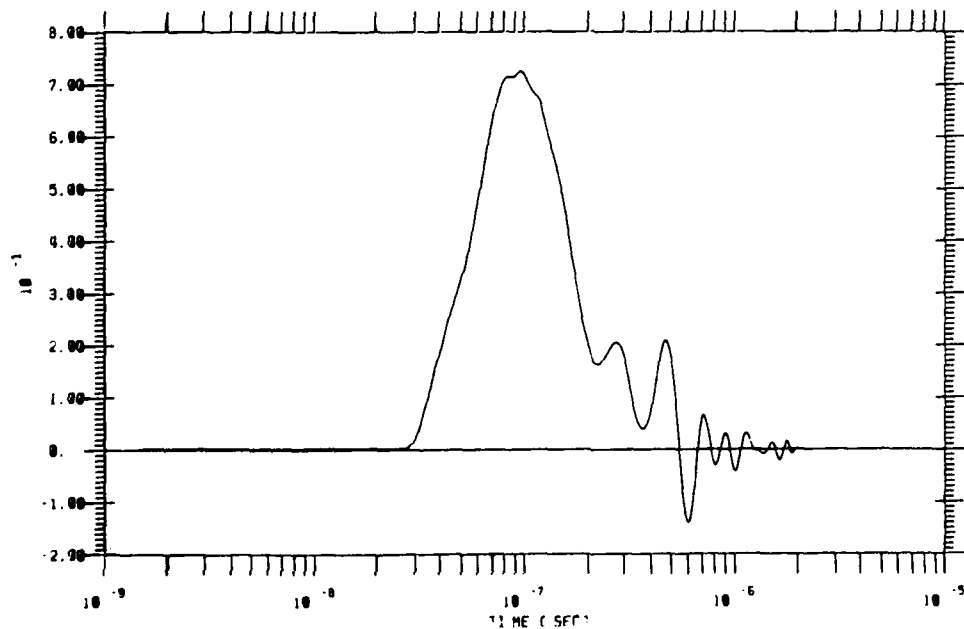


Figure 32b. V_{oc} for Measured Amplitude and Calculated Phase (Horizontal Polarization)

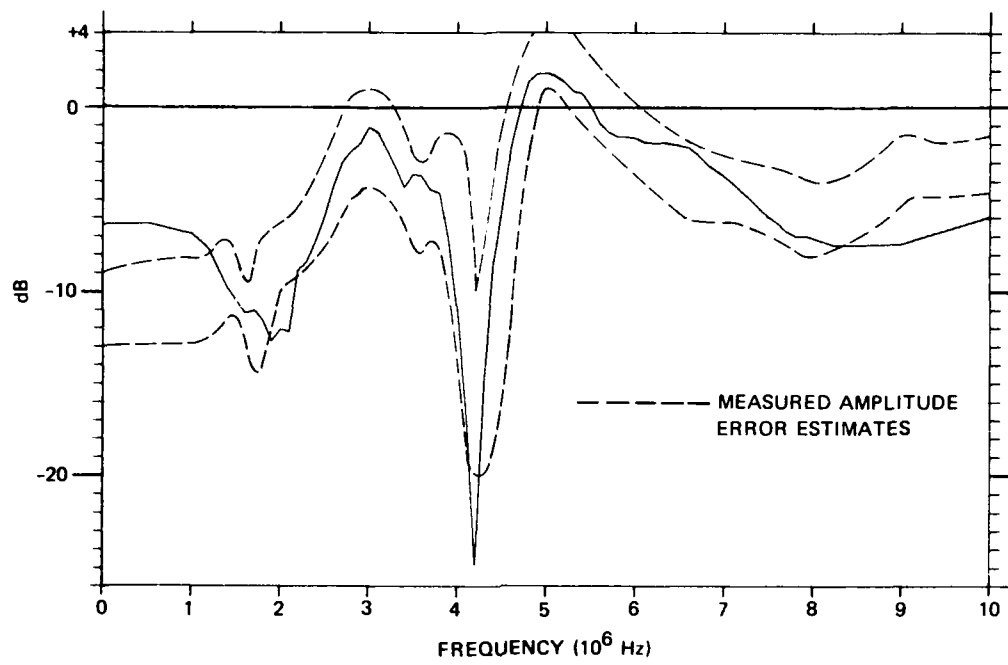


Figure 33a. 45° Polarization Calculated Amplitude (10 MHz)

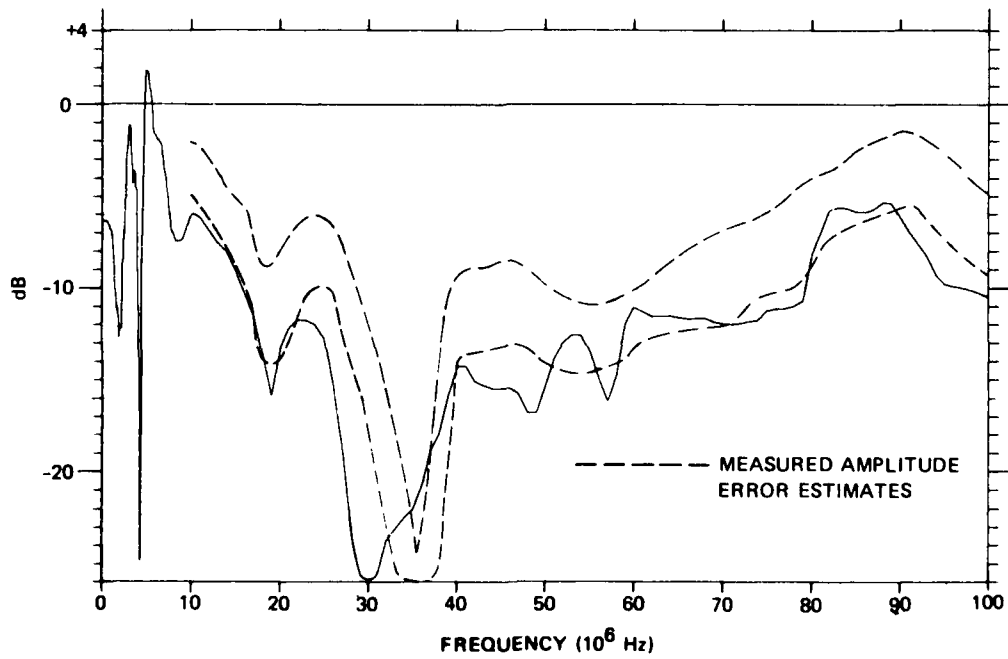


Figure 33b. 45° Polarization Calculated Amplitude (100 MHz)

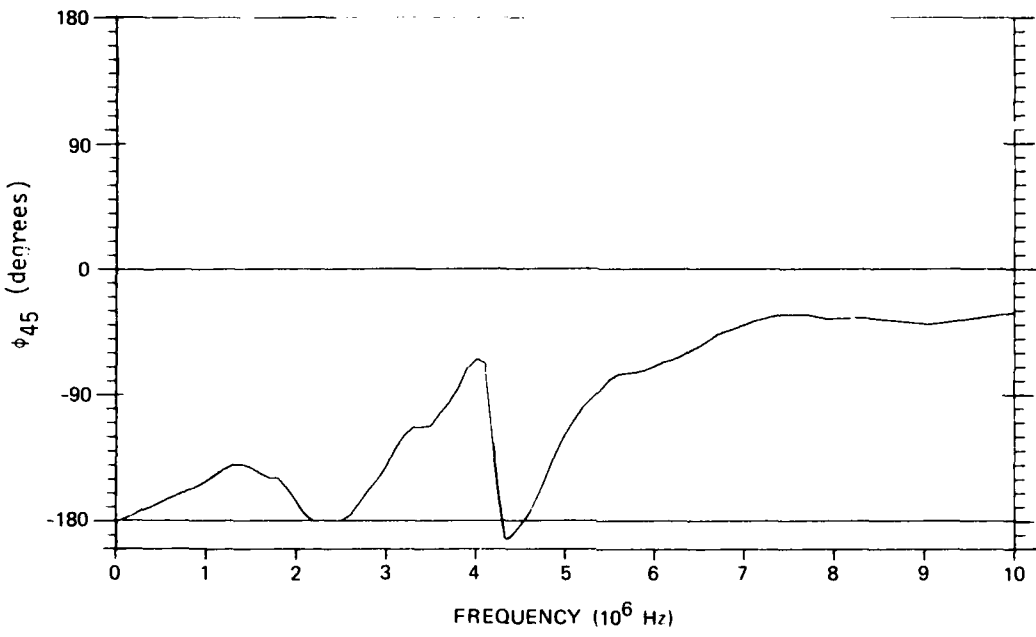


Figure 34a. 45^0 Polarization Calculated Phase

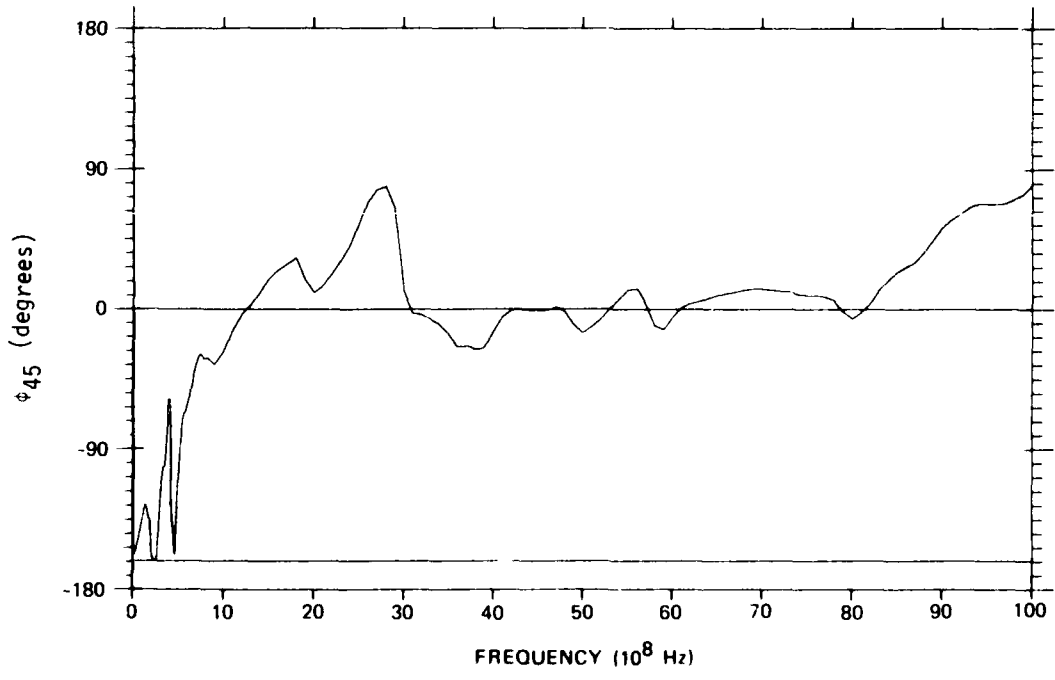


Figure 34b. 45^0 Polarization Calculated Phase

of the shape of the amplitude curve. However, it can be seen that the curve is outside the measured error bounds particularly from 0-1 MHz where it is higher and above 40 MHz where it is lower. Also, note that there is a calculated null on 30 MHz where the measurement shows a null mean 35 MHz. Before showing any conclusions, a brief discussion of combining errors is in order.

If we combine two quantities which have uncertainties associated with each, then the uncertainty on the combined quantity will be at least as large as the individual uncertainty but can be considerably larger. For the curve at hand, let us consider only the uncertainty associated with the amplitude and let the true value of the vertical and horizontal effect heights be:

$$|h_v|_t = |h_v| (1 \pm \epsilon) \quad (62)$$

and

$$|h_h|_t = |h_h| (1 \pm \epsilon) .$$

Now, if both quantities were in error by a constant bias, i.e., if both had the same sign of an ϵ , then it can be shown that

$$|h_{45}|_t \approx |h_{45}| (1 \pm \epsilon)$$

i.e., that the error on the 45° amplitude would be the same as for the horizontal and vertical. However, if the two quantities had different errors, i.e., if the sign of ϵ for the vertical and horizontal were different, then it can be shown that

$$|h_{45}|_t \approx |h_{45}| \left\{ 1 + \cos(45^\circ) \cdot \epsilon \cdot \frac{(|h_v|^2 - |h_h|^2)}{|h_{45}|^2} \right\} . \quad (63)$$

Thus, the error could be larger for the combined value than on the input values.

For example, consider the quasi-static region (0-1 MHz). In this region

$$|h_v| = 0.45 \text{ or } -7 \text{ dB}$$

$$|h_v| = 1.12 \text{ or } 1 \text{ dB}$$

$$|h_{45}| = 0.47 \text{ or } -6.6 \text{ dB.}$$

Let us now consider the measurement accuracy as ± 2 dB ($\sim 20\%$). If the vertical and horizontal were both in error by ± 2 dB, then from Equation 62 the error in $|h_{45}|_t$ would be

$$|h_{45}|_t = -6.6 \text{ dB } \pm 2 \text{ dB.}$$

However, if the errors on the vertical and horizontal data were not the same but at the extremes of the bands, then

$$|h_{45}|_t = -6.6 \text{ dB } \pm 5.4 \text{ dB.}$$

Note that the increase in the combined error as shown in Equation 63 only occurs when the two quantities being combined are near the same magnitude. When one term dominates, then Equation 63 reduces to Equation 62. Thus for the calculated amplitude of the 45° effective height if one considered the additional errors associated with combining two uncertain quantities, the comparisons would be in reasonable agreement.

The phase data shown in Figure 34 has the properties of changing from -180° to 0° discussed previously.

REFERENCES

- B-1. Antenna Effective Length Meaurement, The Boeing Company, Seattle,
Washington, DNA 3798F-1, 2, July 1975.
- B-2. Letter from D. D. Connell (Boeing) to Major W. Adams (DNA) dated
23 September 1975.
- B-3. Antenna Effective Length Measurement, The Boeing Company, Seattle,
Washington, DL80-18878-1, 2, July 1975 (draft).

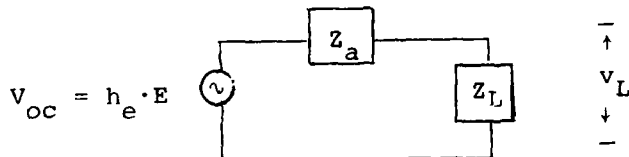
APPENDIX C.

EFFECTIVE HEIGHTS FOR ANTENNAS ON CONDUCTING SURFACES

The effective height of an antenna is a function which relates the free space electric field with the equivalent open circuit voltage that drives the antenna. In the frequency domain, the effective height can be written as:

$$h_e(\omega) = \frac{V_{oc}(\omega)}{E(\omega)} . \quad (64)$$

For a voltage measured across a load, the equivalent circuit would be



where Z_a is the antenna impedance

Z_L is the load impedance

V_L is the voltage drop across the load.

Thus, if one knows the impedances, the load voltage, and the effective height, then one can determine the external field. However, there is a difficulty which has been evident in a number of experimental measurement programs concerning the estimates of antenna effective heights for a monopole over a conducting ground plane.

Electrically, a monopole antenna over a conducting ground plane is equivalent to a center fed dipole in free space. Figure 35 shows this correspondence. Now, for a dipole it is easy to show that in the low frequency limit, quasi-static, $h_e = L$ where $2L$ is the total length of the dipole. Therefore, an incident field of E_0 will produce a voltage drop across the gap of $E_0 \cdot L$. To show this, we note that the voltage drop across both the upper and lower halves of the dipole will be $E_0 \cdot L$. However, since all points in the upper or lower halves must be at the same potential, in the low frequency limit, the potential for the upper half would be $E_0 \cdot L/2$ while for the lower half, it would be $-E_0 \cdot L/2$. Their difference, which represents the voltage drop across the gap, is

$$V_g = (E_o \cdot L/2) + (E_o \cdot L/2)$$

or $V_g = E_o \cdot L.$ (65)

Now, for a monopole for length L over a conducting plane as shown in Figure 35, the electrical situation is the same as for the dipole except the voltage we want is now the voltage drop across half of the gap. Therefore,

$$V_g = \frac{1}{2} (E_o \cdot L) = E_o \cdot L/2. \quad (66)$$

It is important to note that in Equation 65, E_o represents the incident free field; however, in Equation 66 E_o represents the total field. The difference is caused by the presence of the conducting ground plane and may be clarified by the following illustration. Consider a plane wave which is incident on an antenna on a ground plane as shown in Figure 36. The normal component of the incident field is $E_n = E_f \cos \alpha$; however, the normal field on the surface of the conducting ground plane is twice the incident field or in our notation

$$E_o = 2 \cdot E_n = 2 \cdot E_f \cos \alpha. \quad (67)$$

Now, as $\alpha \rightarrow 0$, $E_o = 2 \cdot E_f$. Therefore, if we are defining the effective height to be the relationship between the open circuit voltage and the free field, then for a monopole antenna over a ground plane, the effective height (h_e) at low frequencies is not $L/2$ but L . Thus care must be taken to insure which quantity we are specifying since both of the following equations are true.

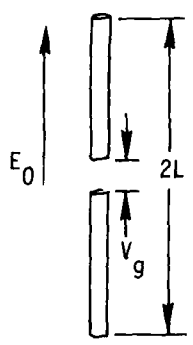
$$V_g = E_o \cdot L/2 \quad (68)$$

and

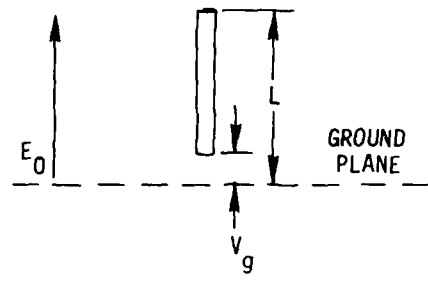
$$V_g = E_f \cdot L.$$

This same situation of the enhancement of the normal component of the electric field occurs when the antenna is on a conducting cylinder. Consider the geometry shown in Figure 37.

For low frequencies we can approximate the field along the antenna as



DIPOLE



MONPOLE OVER GROUND PLANE

Figure 35. Dipole and Monopole Over Ground Plane

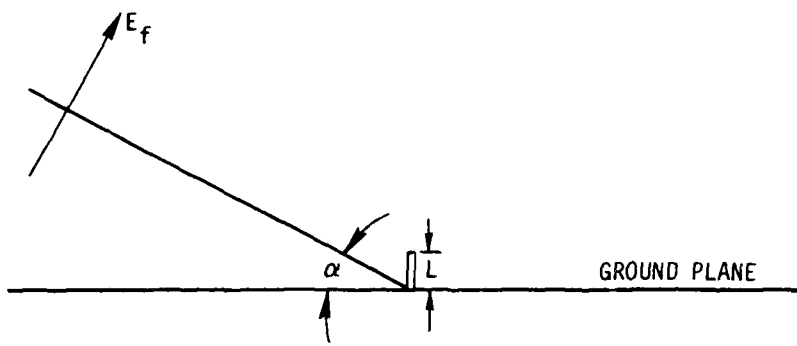


Figure 36. Incident Field on a Monopole Antenna

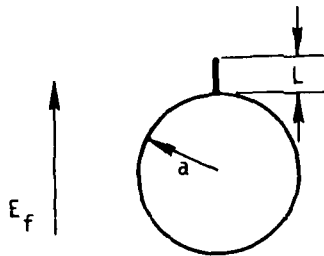


Figure 37. Incident Field on an Antenna Mounted on a Cylinder

$$E_o \approx E_f \left(1 + \frac{a^2}{r^2}\right) . \quad (69)$$

Thus, the open circuit voltage for $L/a < 1$ would be approximately

$$V \approx E_f \cdot L \left(1 - \frac{L}{2a}\right) \quad (70)$$

and the effective height is

$$h_e \approx L \left(1 - \frac{L}{2a}\right) . \quad (71)$$

Again, the effective height is larger than the value of $L/2$ commonly attributed to a monopole over a ground plane with this difference or "enhancement" caused by the difference between a free field and the normal field on a conducting surface.

One final point should be made concerning the effective height for an antenna on a finite length conducting cylinder. Again, we will only consider the low frequencies. As shown in Figure 38, for an incident vertical electric field, the charge distribution on the cylinder caused by the field enhances the local normal field. For an antenna in the center of the cylinder, the net field created by the charges on either side will be aligned along the antenna in the center of the cylinder, the net field created by the charges on either side will be aligned along the antenna and then one would expect an effective height as given by Equation 71. However, as the antenna is moved toward either end, the charge distribution is no longer symmetric; and thus, the net field direction is not aligned with the antenna and the effective height will be less than that given in Equation 71.

If there is a horizontal component of the incident field as shown in Figure 39, then the charge distribution will create electric fields with the polarization shown. For an antenna at the symmetric center of the charge distribution, the electron field will be perpendicular to the antenna and there will be no coupling. However, for an antenna located near either end, the electron field will have a component along the antenna but the sign of the induced voltage will change from one end to the other.

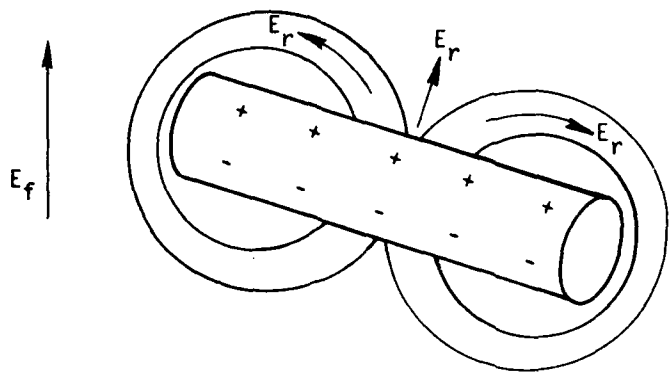


Figure 38. Electrostatic Field from a Finite Cylinder in a Vertical Field

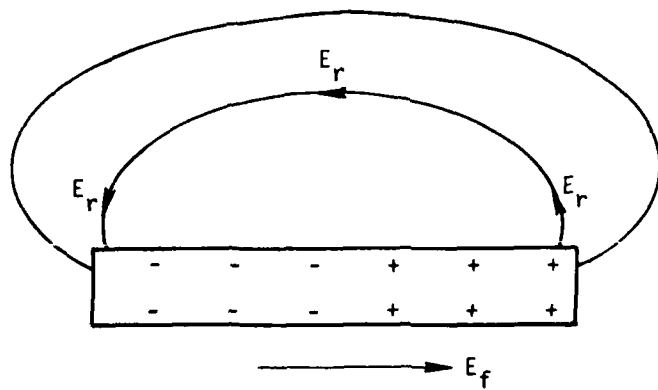


Figure 39. Electrostatic Field from a Finite Cylinder in a Horizontal Field

DISTRIBUTION LIST

DEPARTMENT OF DEFENSE

Director
 Armed Forces Radiobiology Research Institute
 Defense Nuclear Agency
 National Naval Medical Center
 ATTN: RPC

Assistant to the Secretary of Defense
 Atomic Energy
 Department of Defense
 ATTN: Staff Asst. (R&D)

Director
 Defense Advanced Rsch. Proj. Agency
 ATTN: AD/F&PS
 ATTN: Technical Library

Director
 Defense Civil Preparedness Agency
 Assistant Director for Research
 ATTN: PO(SE)
 ATTN: RE(EO)
 ATTN: Admin. Officer
 ATTN: TS AED

Defense Communication Engineer Center
 ATTN: Code R720, C. Stansberry
 ATTN: Code R123, Tech. Lib.
 ATTN: Code R400

Director
 Defense Communications Agency
 ATTN: Code 930, Monte I. Burgett, Jr.
 ATTN: CCTC/C672

Defense Documentation Center
 Cameron Station
 12 cy ATTN: TC

Commander
 Defense Electronic Supply Center
 ATTN: Ross V. Doughty

Director
 Defense Intelligence Agency
 ATTN: RDS-3A4, Pomponio Plaza
 ATTN: RDS-3A

Director
 Defense Nuclear Agency
 ATTN: RAEV
 3 cy ATTN: TITL, Tech. Library
 ATTN: TISI, Archives
 ATTN: RATN
 ATTN: STVL
 ATTN: DDST

Dir. of Defense Rsch. & Engineering
 Department of Defense
 ATTN: S&SS (OS)
 ATTN: G. Barse

DEPARTMENT OF DEFENSE (Continued)

Commander
 Field Command
 Defense Nuclear Agency
 ATTN: FCPR
 ATTN: FCSM-F3/CDR Smith
 ATTN: FCLMC

Director
 Interservice Nuclear Weapons School
 ATTN: Document Control

Director
 Joint Strat. Target Planning Staff, JCS
 ATTN: STINFO, Library

Chief
 Livermore Division, Field Command, DNA
 Lawrence Livermore Laboratory
 ATTN: FCPLR

National Communications System
 Office of the Manager
 ATTN: NCS-TS, Charles D. Bodson

Director
 National Security Agency
 ATTN: T1213
 ATTN: Orlando Van Gunten, R-425
 ATTN: Technical Library
 ATTN: T412

OJCS/J-3
 ATTN: J-3

DEPARTMENT OF THE ARMY

Director
 BMD Advanced Tech. Center
 Huntsville Office
 ATTN: Tech. Lib.

Commander
 BMD System Command
 ATTN: Technical Library
 ATTN: BDMSC-TEN, Noah J. Hurst

Dep. Chief of Staff for Rsch. Dev. & Acq.
 Department of the Army
 ATTN: DAMA-CSM-N, 1TC G, Ogden

Commander
 Harry Diamond Laboratories
 ATTN: DRXDO-NP, Francis N. Wimenitz
 ATTN: DRXDO-RGC
 ATTN: DRXDO-T1, Tech. Lib.
 ATTN: DRXDO-TD
 ATTN: DRXDO-EM, R. E. McCoskey
 ATTN: DRXDO-TE, R. B. Oswald
 ATTN: DRXDO-EM-1
 ATTN: DRXDO-EM-2
 ATTN: DRXDO-EM-3
 ATTN: DRXDO-EM-4
 ATTN: DRXDO-EM-5

DEPARTMENT OF ARMY (Continued)

Commander
Picatinny Arsenal
ATTN: Technical Library
ATTN: SMUPA-ND-D-C-2
ATTN: SARPA-ND-C-E, Amina Nordio
ATTN: SMUPA-ND-W

Commander
US Army Armor Center
ATTN: Technical Library

Director
US Army Ballistic Research Labs.
ATTN: DRSTE-EL
ATTN: DRDAR-BLE

Commander
US Army Comm.-Elec. Engrg. Instal. Agy.
ATTN: CCC-PRSO-S

Commander
US Army Communications Command
ATTN: CC-OPS-OS
ATTN: CC-OPS-PD

Commander
US Army Communications Command
ATTN: ATSI-CD-MD

Chief
US Army Communications Sys. Agency
ATTN: CCM-RD-T CCM-AD-SV

Commander
US Army Electronics Command
ATTN: DRSEL-CT-HDK, Abraham E. Cohen
ATTN: DRSEL-GG-TD, W. R. Werk
ATTN: DRSEL-NL-RO, R. Brown

Division Engineer
US Army Engineer Div. Huntsville
ATTN: HNDED-SR

Commander in Chief
US Army Europe & Seventh Army
ATTN: Technical Library

Director
US Army Materiel Sys. Analysis Acty.
ATTN: Technical Library

Commander
US Army Missile Command
ATTN: DRSMI-RGD, Vic Ruwe
ATTN: DRSMI-RGP, Hugh Green
ATTN: DRCPM-PE-EA, Wallace O. Wagner

Commander
US Army Mobility Equip. R & D Center
ATTN: Technical Library

Commander
US Army Nuclear Agency
ATTN: Colonel Deverill
ATTN: ATCN-W, LTC Leonard A. Sluga
ATTN: Tech. Lib.

DEPARTMENT OF THE ARMY (Continued)

Commander
US Army Security Agency
ATTN: Technical Library

Commander
US Army Test & Evaluation Command
ATTN: DRSTE-EL, Richard I. Kolchin
ATTN: Technical Library

Commander
US Army Training & Doctrine Command
ATTN: Tech. Library

Commander
White Sands Missile Range
ATTN: Technical Library
ATTN: STEWS-TE-NT, Marvin P. Squires
ATTN: STEWS-TE-AN/A. De La Paz

DEPARTMENT OF THE NAVY

Officer-in-Charge
Civil Engineering Laboratory
Naval Construction Battalion Center
ATTN: Technical Library

Commander
Naval Air Systems Command
Headquarters
ATTN: Tech. Lib.

Commander
Naval Electronic Systems Command
Naval Electronic Systems Command Hqs.
ATTN: PME 117-215A, Gunter Brunhart
ATTN: Tech. Lib.

Commanding Officer
Naval Intelligence Support Center
ATTN: Technical Library

Commander
Naval Ocean Systems Center
ATTN: Technical Library
ATTN: Code 3100, E. E. McCown
ATTN: Code 2200, Verne E. Hildebrand
ATTN: Code 2400, S. W. Lichtman

Superintendent (Code 1424)
Naval Postgraduate School
ATTN: Code 2124, Tech. Rpts. Librarian

Director
Naval Research Laboratory
ATTN: Code 2600, Tech. Lib.
ATTN: Code 2627, Doris R. Folen
ATTN: Code 4004, Emanuel L. Brancato
ATTN: Code 6631, James C. Ritter

Officer-in-Charge
Naval Surface Weapons Center
ATTN: Code 223, L. Libello
ATTN: Code WR43
ATTN: Code WA501, Navy Nuc. Progms. Off.
ATTN: Code 431, Edwin R. Rathburn
ATTN: Code WA50, John H. Malloy

DEPARTMENT OF THE NAVY (Continued)

Commander
Naval Surface Weapons Center
Dahlgren Laboratory
ATTN: Technical Library

Commanding Officer
Naval Weapons Evaluation Facility
ATTN: Lawrence R. Oliver
ATTN: Code ATG, Mr. Stanley

Commanding Officer
Naval Weapons Support Center
ATTN: Code 7024, James Ramsey
ATTN: Technical Library

Director
Strategic Systems Project Office
Navy Department
ATTN: NSP-43, Tech. Lib.
ATTN: NSP-230, David Gold
ATTN: SP 2701, John W. Pitsenberger

DEPARTMENT OF THE AIR FORCE

AF Weapons Laboratory, AFSC
ATTN: ELP
ATTN: ELA, J. P. Castillo
ATTN: CA
ATTN: ELXT
ATTN: NT, Carl E. Baum
ATTN: NT
ATTN: SUL

Commander
Air University
ATTN: AUL/LSE-70-250

Commander
ASD
ATTN: ENFTV

Headquarters
Electronic Systems Division/YS
ATTN: YSEV

Commander
Foreign Technology Division, AFSC
ATTN: ETD, B. L. Ballard

Commander
Ogden Air Logistics Center
ATTN: MMEDO, Leo Kidman
ATTN: OO-ALC/MMETH, P. W. Berthel
ATTN: Major Ronald Blackburn

Commander
Rome Air Development Center, AFSC
ATTN: TSLD

SAMSO/IN
ATTN: IND, I. J. Judy

SAMSO/MN
ATTN: MNNH, Major M. Baran
ATTN: MNNH, Captain R. L. Lawrence

SAMSO/YA
ATTN: YAPC

DEPARTMENT OF THE AIR FORCE (Continued)

Commander in Chief
Strategic Air Command
ATTN: NRI-STINFO, Library
ATTN: DEL
ATTN: Garnet E. Matzke
ATTN: XPFS, Major Brian G. Stephan

ENERGY RESEARCH & DEVELOPMENT ADMINISTRATION

University of California
Lawrence Livermore Laboratory
ATTN: Hans Kruger, I-96
ATTN: Librarian
ATTN: Terry R. Donich, I-96

Los Alamos Scientific Laboratory
ATTN: Doc. Con. for Clarence Benton

Sandia Laboratories
ATTN: Doc. Con. for Org. 9353, R. L. Parker

US Energy Rsch. & Dev. Admin.
Albuquerque Operations Office
ATTN: Doc. Con. for Tech. Library

OTHER GOVERNMENT AGENCIES

Central Intelligence Agency
ATTN: RD/SI, Rm. 5G48, Hq. Bldg. for OSI/
NED/NWB

Administrator
Defense Electric Power Admin.
Department of the Interior
ATTN: L. O'Neill

Department of Transportation
Federal Aviation Administration
Headquarters Sec. Div. ASF-300
ATTN: Sec. Div. ASF-300

DEPARTMENT OF DEFENSE CONTRACTORS

Aerospace Corporation
ATTN: Julian Reinheimer
ATTN: C. B. Pearlston
ATTN: Library
ATTN: Irving M. Garfunkel

Agbabian Associates
ATTN: Library

Battelle Memorial Institute
ATTN: Technical Library

The BDM Corporation
ATTN: J. H. Neighbors
ATTN: Technical Library

The BDM Corporation
ATTN: Tech. Lib.

The Boeing Company
ATTN: Howard W. Wicklein, MS 17-11
ATTN: Aerospace Library
ATTN: D. F. Isbell
ATTN: David Kemle

DEPARTMENT OF DEFENSE CONTRACTORS (Continued)

Booz-Allen & Hamilton, Inc.
ATTN: Raymond J. Chrisner
ATTN: Tech. Lib.

Brown Engineering Company, Inc.
ATTN: John M. McSwain, MS 18
ATTN: Tech. Lib., MS12, P. Shelton

Burroughs Corporation
Federal & Special Systems Group
ATTN: Angelo J. Mauriello
ATTN: Tech. Lib.

Calspan Corporation
ATTN: Technical Library

Charles Stark Draper Laboratory, Inc.
ATTN: Kenneth Fertig
ATTN: Tech. Lib.

Computer Sciences Corporation
ATTN: Tech. Lib.

Computer Sciences Corporation
ATTN: Alvin T. Schiff

Control Data Corporation
ATTN: Jack Meehan

Cutler-Hammer, Inc.
All Division
ATTN: Central Tech. Files, Anne Anthony

Dikewood Industries, Inc.
ATTN: L. Wayne Davis
ATTN: Tech. Lib.

EG&G, Inc.
Albuquerque Division
ATTN: Technical Library

ESL, Inc.
ATTN: Technical Library

Ford Aerospace & Communications Operations
ATTN: L. R. Poncelet, Jr.
ATTN: Tech. Info. Section
ATTN: Ken G. Attinger

Garrett Corporation
ATTN: Tech. Lib.

General Electric Company
TEMPO-Center for Advanced Studies
ATTN: DASIAC

General Research Corporation
ATTN: Tech. Info. Office

Georgia Institute of Technology
Georgia Tech Research Institute
ATTN: R. Curry

GTE Sylvania, Inc.
Electronics Systems GRP-Eastern Div.
ATTN: James A. Waldon
ATTN: Charles A. Thornhill, Librarian
ATTN: Leonard L. Blaisell

DEPARTMENT OF DEFENSE CONTRACTORS (Continued)

GTE Sylvania, Inc.
ATTN: Comm. Syst. Div., Emil P. Motchok
ATTN: A S M Dept., S. E. Perlman
ATTN: H & V Group, Mario A. Nureforsa

Harris Corporation
Harris Semiconductor Division
ATTN: T. L. Clark, MS 4040
ATTN: Tech. Lib.
ATTN: Carl F. Davis, MS 17-220
ATTN: Wayne F. Abare, MS 16-111

Honeywell Incorporated
Avionics Division
ATTN: Technical Library

IIT Research Institute
ATTN: Jack E. Bridges
ATTN: Technical Library
ATTN: Irving N. Mindel

Institute for Defense Analyses
ATTN: IDA Librarian, Ruth S. Smith

IRT Corporation
ATTN: Technical Library
ATTN: R. L. Mertz

Jaycor
ATTN: Eric P. Kenas
ATTN: Ralph H. Stahl

Jaycor
ATTN: Catherine Turesko
ATTN: Robert Sullivan

Johns Hopkins University
Applied Physics Laboratory
ATTN: Tech. Lib.

Kaman Sciences Corporation
ATTN: Library
ATTN: Donald B. Bryce
ATTN: Jerry L. Lubell
ATTN: Albert P. Bridges
ATTN: W. Lester Klein
ATTN: L. R. Curry
ATTN: Walter F. Ware

Litton Systems, Inc.
AMFOM Division
ATTN: Tech. Lib.

Lockheed Missiles & Space Company, Inc.
ATTN: George F. Peatly, P. S1-14
ATTN: Samuel L. Fairbank, Dept. 66-85
ATTN: L-653, Dept. S1-20
ATTN: L. Rossi, Dept. S1-64
ATTN: Benjamin L. Finney, Dept. S1-1
ATTN: Technical Library

M.I.T. Lincoln Laboratory
ATTN: Leonor Touchling, Librarian A-082

Martin Marietta Corporation
Denver Division
ATTN: Ben L. Graham, MS 10-534
ATTN: Ray F. McKee, Research Lib., 6617

DEPARTMENT OF DEFENSE CONTRACTORS (Continued)

Maxwell Laboratories, Inc.
ATTN: Tech. Lib.

Mission Research Corporation
ATTN: Daniel F. Higgins
ATTN: William C. Hart
ATTN: Tech. Lib.

Mission Research Corporation
ATTN: David E. Merewether
ATTN: Tech. Lib.
ATTN: Larry D. Scott

Mission Research Corporation-San Diego
ATTN: V. A. J. Van Lint

The Mitre Corporation
ATTN: M. E. Fitzgerald
ATTN: Library

Northrop Corporation
Northrop Research & Technology Center
ATTN: Library

Northrop Corporation
Electronic Division
ATTN: Vincent R. DeMartino
ATTN: Lew Smith
ATTN: Tech. Lib.

Physics International Company
ATTN: Doc. Con. for Tech. Lib.

R & D Associates
ATTN: William R. Graham, Jr.
ATTN: S. Clay Rogers
ATTN: Charles Mo
ATTN: Technical Library
ATTN: William J. Parsons
ATTN: Gerald W. Schaefer

RCA Corporation
Government Systems Division
Astro Electronics
ATTN: Tech. Lib.

Rockwell International Corporation
ATTN: Technical Library
ATTN: K. F. Bell
ATTN: J. L. Monroe, Dept. 243-027, Div. 031
ATTN: Donald J. Stevens, FA70
ATTN: James E. Bell, HA10

Science Applications, Inc.
ATTN: Technical Library

DEPARTMENT OF DEFENSE CONTRACTORS (Continued)

Science Applications, Inc.
Huntsville Division
ATTN: Noel R. Byrn
ATTN: Tech. Lib.

Science Applications, Inc.
ATTN: J. Roger Hill

Sidney Frankel & Associates
ATTN: Sidney Frankel

Stanford Research Institute
ATTN: Arthur Lee Whitson
ATTN: Philip J. Dolan
ATTN: Mel Bernstein

Systems, Science & Software, Inc.
ATTN: Tech. Lib.

Systems, Science & Software, Inc.
ATTN: Technical Library

Texas Instruments, Inc.
ATTN: Tech. Lib.
ATTN: Donald J. Manus, MS 72

TRW Defense & Space Sys. Group
2 cy ATTN: Robert M. Webb, RI-2410
8 cy ATTN: Tech. Info. Center/S-1930
ATTN: Aaron H. Narevsky, RI-2144

TRW Defense & Space Sys. Group
San Bernardino Operations
ATTN: F. B. Fay

Vector Research Associates
ATTN: W. A. Radasky

Westinghouse Electric Corporation
Advanced Energy Systems Div.
ATTN: Tech. Lib.